APPLYING A MODEL OF OROGRAPHIC PRECIPITATION TO IMPROVE MASS BALANCE MODELING OF THE JUNEAU ICEFIELD

By

Aurora Roth, B.A.

A Thesis Submitted in Partial Fulfillment of the Requirements

for the Degree of

MASTER OF SCIENCE

in

Geophysics

University of Alaska Fairbanks

December 2016

APPROVED:

Dr. Regine Hock, Committee Chair
Dr. Martin Truffer, Committee Member
Dr. Andy Aschwanden, Committee Member
Dr. Paul McCarthy, Chair
Department of Geosciences
Dr. Paul Layer, Dean
College of Natural Science and Mathematics
Dr. Michael Castellini, *Dean of the Graduate School*

Abstract

Mass loss from glaciers in Southeast Alaska is expected to alter downstream environmental conditions such as streamflow patterns, riverine and coastal ecological systems, and ocean properties. To investigate these potential changes under future climate scenarios, accurate climate data are needed to drive glacier mass balance models. However, assessing and modeling precipitation in mountainous regions remains a major challenge in glacier mass balance modeling. We have used a linear theory of orographic precipitation model (LT model) to downscale precipitation from both the Weather Research and Forecasting (WRF) model and the European Centre for Medium-Range Weather Forecasts interim reanalysis (ERA-Interim) to the Juneau Icefield, one of the largest icefields in North America (4149 km^2), over the period 1979–2013. The LT model is physically-based, combining airflow dynamics and simple cloud microphysics to simulate precipitation in complex terrain. Cloud microphysics is parameterized as a function of user-defined snow and rain fall speeds which are then used to calculate the cloud time delay, τ, at every time step. We established a model reference run using literature values of snow fall speed and rain fall speed. The model was run using a 1 km digital elevation model and 6 hour timesteps. Due to a lack of precipitation observations, we validated the model with point net accumulation observations along an 8.5 km transect on Taku glacier, one of the largest and best-studied outlet glaciers of the icefield. The observations occurred in late July of 1998, 2004, 2005, 2010, and 2011. We extracted the snow portion from the modeled precipitation and accounted for melt using a temperature-index model prior to comparing results to the observations. The latter was necessary since the observations were taken when substantial melt of the winter snow cover had occurred. The results of the reference run show reasonable agreement with the available glaciological observations (r^2 = 0.89). We assessed the LT model results in terms of the icefield-wide average winter (October-March) precipitation amount and its spatial pattern for the 1979-2013 time period. To express the latter we calculated a precipitation index map where each grid cell of average winter precipitation was divided by the icefield-wide spatial mean. The downscaled precipitation pattern produced by the LT model is consistent with the expected orographic precipitation pattern with substantially reduced precipitation on the eastern lee-side portion of the icefield, a pattern that is absent in the coarse resolution WRF and ERA-Interim precipitation fields. To investigate the robustness of the LT model results, we performed a series of sensitivity experiments varying the LT model parameters of snow fall speed and rain fall speed, as well as the horizontal resolution of the underlying grid, and the climate input data. The precipitation pattern produced by the LT model was stable regardless of the parameter combination, horizontal resolution, and climate input data, but the precipitation amount varied strongly with these factors. For the range of snow fall speeds tested and holding all other parameters constant, the average winter precipitation spatial mean varied from 2.5 m to 4.4 m. We were unable to constrain the precipitation amount due to the scarcity of validation data. However,

given the stability of the winter precipitation pattern produced by the LT model, we suggest a winter precipitation index map calculated from the LT model reference run results be used in combination with a distributed mass balance model for future mass balance modeling studies of the Juneau Icefield. More observations of total precipitation are needed to further validate the precipitation pattern of the LT model results, constrain the model parameters, and improve the estimation of total precipitation amounts by the LT model. We suggest three locations for potential weather stations that would be most beneficial for validating LT model results. The LT model could be applied to other regions in Alaska and elsewhere with strong orographic effects for improved glacier mass balance modeling and/or hydrological modeling.

Table of Contents

Page

Page

List of Figures

Page

List of Tables

Acknowledgements

First and foremost, I would like to thank my advisor, Dr. Regine Hock. Regine has been an incredible mentor and supporter for much longer than just the time of this degree, and I really can't say enough here that would express my gratitude for her mentorship. She has steered me through many academic challenges and has helped to make sure that I stay excited about science. Regine has had to put up with my procrastination and perfectionism (not an ideal combination) and has spent many late hours with me going over specific sentences in a proposal or a paper, and the writing is always much, much better afterward. Even when she was at her busiest, she always found time to answer a question, read a paragraph, or just check in. I have developed tremendously towards becoming a well-rounded, careful scientist with her guidance. I am grateful for her supporting my desires to galavant off to faraway lands and for her role in helping me experience Norwegian ski trails and brunost (brown cheese). I have realized how important it is to have an advisor that is just as excited about a scientific idea as she is about skiing fresh snow at Sölden (or Skiland: The Sölden of Fairbanks). I am inspired by Regine's dedication to building the glaciers group community through potlucks and chocolate cake. My graduate experience would have been very different without that sense of community (and chocolate cake).

I owe many thanks to my committee members Dr. Andy Aschwanden and Dr. Martin Truffer, who also put up with my procrastination and were an integral part of this thesis journey. Andy always made time to answer my questions about netcdf and nco (though I may have had to exchange some chocolate for that), and his perspective on the LT model as he has become an expert has been invaluable. Martin contributed helpful advice and perspective, and I always left every committee meeting mulling over an idea or direction that he pointed me in. He suggested creating an adjoint model for the LT model, and I hope to have time in the future to explore this! Additionally, Martin invited me to join his team for spring field work on Taku Glacier and I am incredibly thankful for that. At a time when I was struggling with the model, I was able to get out of the office and remember why I love glaciers, ice, and snow. Every day in the field I learned something new about science and myself. We even got in a few turns and a few bites of fondue and raclette too! (I will never have a better field work food experience).

Thank you also to my collaborators Dr. Thomas Schuler at the University of Oslo and Dr. Peter Bieniek at the International Arctic Research Center at University of Alaska Fairbanks (UAF). Thomas provided the original code of the LT model and helped get this whole project rolling. He made time to answer all my questions, big and small, as I was navigating the MATLAB maze. I am grateful for the opportunity that I had to spend time in Oslo working with the glaciers group there. Peter provided me with the climate data that he generated and was a valuable source of information and advice. It was always nice to know that this thesis was of interest and relevant to the downscaling group.

He and Dr. Uma Bhatt made time to attend various presentations that I gave and provided helpful feedback. Additionally, Mauri Pelto graciously provided the net accumulation observations on Taku Glacier used here as model validation data.

I must thank the organizations that allowed me to buy vegetables, pay rent, and travel. The Resilience and Adaptation Program (RAP) at UAF generously provided 1.5 years of funding as well as a network of interdisciplinary graduate students and training in interdisciplinary research and communication. The Glaciology Exchange program (GlacioEx) funded by the Norwegian Center for International Cooperation in Education (SIU) paid for all expenses during my exchange in Norway. The High North Fellowship paid for my tuition and board while I studied at the University Centre in Svalbard, Norway. The Alaska Center for Climate Assessment and Policy (ACCAP) at UAF provided one year of support. Many thanks are due to Dr. Sarah Trainor for the funding connection and support from ACCAP.

The Glaciers Group at the Geophysical Institute is like no other and has contributed immensely to my development as a scientist and human being. Thank you to all the professors, faculty, and emeritus for lunch time banter, asking thoughtful questions in seminars, and for sharing your inspiration and passion. Thank you to all my fellow graduate students for pep talks, chocolate, adventures, car borrowing, and inspiration (scientific and in life). Some specific shout outs include: Christian Kienholz, office mate, for often being at the office on weekends with me, making that much less miserable, sharing in day to day triumphs and complaints, and for being a GIS wizard. Joanna Young and Chris Carr for being older and wiser mentors in so many ways. Jenna Zechmann for always being up for adventure, finding some snow to ski, or a river to float. Doug Brinkerhoff for always providing a balanced perspective on life and work, patiently answering all my questions in Foundations of Geophysics class, and being a generally chill dude to play music with and ski with. Jessica Mejia for being in the office at the wee hours of the night with me working on homework and lamenting about work. Emilie Sinkler for being my new office mate and Antarctica medical process buddy, and Matvey Debolskiy for joining me on the PhD comps adventure.

I relied on an incredible support network of friends and family these past two years. An enormous hug and many thanks to the friends, near and far, that I shared a coffee or beer with, called, or emailed. To list you all here would take up too much space, but you know who you are. They reminded me of why this was important to me, and they kept me grounded. A special shout out to my Hidden Hill family who saw me at my worst and always had a hug and some delicious food ready. Finally, many thanks to my parents. They do an incredible job of letting me make my own mistakes even though they've walked this path and have guided many students through it. It's a very special thing to have parents who want to hear you talk about how you spent several hours debugging code. They understand the triumphs and challenges of academia and are always ready with love.

Chapter 1
Introduction

1.1 Motivation

The Juneau Icefield in the northern Coast Mountains of southeast Alaska is one of the largest icefields in North America and is intimately connected to the ecosystems and communities of the area (O'Neel et al., 2015). Glaciers throughout southeast Alaska are losing mass at some of the highest rates on Earth and this mass loss is expected to continue in this century (Radić et al., 2014). Mass loss from the Juneau Icefield will not only alter the geography and landscape of the immediate area, but will also impact physical and biological processes of downstream ecosystems as glacier runoff patterns change (Hood and Berner, 2009; O'Neel et al., 2015).

The rugged and complex terrain of the Juneau Icefield region poses challenges for modeling the climate and glaciers in the region. Ziemen et al. (2016) was the first modeling study to make projections for the Juneau Icefield region using physically-based flow modeling rather than simple scaling for empirical methods employed by previous regional projections applied to all of Alaska (eg. Radić and Hock (2011); Huss and Hock (2015)). Results indicated a 58-68% volume loss of the icefield in 2099 compared to 2010. However, when attempting to calibrate model parameters for the hindcast period (1979-2013), Ziemen et al. (2016) were unable to match modeled results to observations. This was attributed to the 20 km grid size of the downscaled input climate data being unable to resolve the steep precipitation gradient across the icefield caused by orographic effects. Using newly introduced tuning parameters to adjust the pattern and amount of the precipitation input, they were able to match their model results to the available mass balance observations. While this method employed by Ziemen et al. (2016) is effective given the limitations of the climate data, it is not an ideal solution because it lacks physical basis. A better downscaling approach is needed to account for the spatial variability of precipitation over the Juneau Icefield.

1.2 Scaling Precipitation Data

Precipitation data is a required input for most glacier mass balance models. Distributed mass balance models require precipitation input for every grid cell in the model domain at resolutions ranging from tens of meters to tens of kilometers depending on the area and characteristics being investigated and the model type. Precipitation at the mass balance model resolution must be derived from individual points or from a spatially distributed global or regional climate model with a coarse resolution (20 km - 100 km resolution). The mismatch between the spatial scale of the precipitation data and spatial resolution of a given distributed mass balance model must be addressed before the precipitation data can be used as input.

There are two main approaches for creating precipitation input at the appropriate scale for glacier

mass balance modeling. The first approach involves extrapolating point data, either one or multiple points, across an entire domain. Point data can be observations from a weather station within or near the glacier mass balance model domain or they can be a grid cell from a coarse (~100 km) global climate model where one cell encompasses the glacier mass balance model domain. In either case, one or multiple point values of precipitation are related to other characteristics of the model domain, usually elevation, so that distinct precipitation values are calculated for every cell in the model domain. The most simple approach uses a vertical lapse rate that expresses precipitation as a linear function of elevation (Hock and Holmgren, 2005). This is a common approach for glaciological applications that consider an individual glacier where regional scale variations in precipitation are unimportant.

A more sophisticated approach appropriate for regional scale precipitation fields from point observations is the statistical downscaling, such as the method used by the Parameter-elevation Relationships on Independent Slopes Model (PRISM) (Daly et al., 1994). PRISM uses historic statistical relationships between large scale conditions and local effects to develop a precipitation dataset that accounts for physiographic factors that influence climate patterns at a scale of 1 km or greater. However, in the case of Alaska and other data sparse regions, applications of statistical downscaling are limited by the availability of high resolution and long term observations needed to compute the necessary statistics (Bieniek et al., 2016).

The third approach for creating precipitation input at the appropriate scale for glacier mass balance modeling uses coarsely gridded output from a global climate model (~100 km resolution) to drive a dynamic, physically based regional climate model at a higher resolution (5 km - 50 km resolution) allowing for more complex topography and atmospheric processes to be accounted for. This approach is called dynamic downscaling. While dynamic downscaling is more appropriate for data sparse regions, it is significantly more computationally intensive than statistical downscaling. Recently, a regional climate data set (Bieniek et al., 2016) was produced for all of Alaska at ~20 km spatial and hourly temporal resolution through dynamic downscaling of the ERA-Interim reanalysis, a global climate data product from the European Centre for Medium-Range Weather Forecasts (ECMWF) (Dee et al., 2011). The Weather Research and Forecasting (WRF) Model (Skamarock et al., 2008) was the regional climate model used in the downscaling process. While this dataset is the best available climate data product for all of Alaska, the ~20 km resolution does not meet the needs of glacier mass balance modeling. Additionally, the ~20 km resolution does not adequately represent complex, mountainous terrain and this impacts meteorological variables that are sensitive to topography, often underestimating precipitation amount and simplifying the spatial variability of precipitation. Further downscaling is needed to meet the needs of glacier modeling.

1.3 The LT Model: An Intermediate Approach

Rather than these two extremes, a linear theory of orographic precipitation model (hereafter referred to as the LT model) is a physically-based downscaling method of intermediate complexity that captures the orographic precipitation pattern necessary for improved performance of mass balance models (Jarosch et al., 2012; Ziemen et al., 2016). The LT model has been explored and applied as a precipitation downscaling technique in numerous mountainous regions, but has only been used for direct glaciological applications in Iceland (Crochet et al., 2007; Jóhannesson et al., 2007; Crochet, 2012), Norway (Schuler et al., 2008), and Western Canada (Jarosch et al., 2012). The LT model considers 3D airflow dynamics with simple parameterizations of cloud microphysics. Complex non-linear atmospheric dynamics that contribute to the computational intensity of regional climate models are reduced using linear mountain wave theory. Some observations are needed to calibrate the few LT model parameters, but the spatial resolution and historical record of observations required by statistical downscaling methods is not necessary.

1.4 Objectives

The purpose of this study is to evaluate the capacity of the LT model to provide accurate winter precipitation fields of the Juneau Icefield with the ultimate goal to improve mass balance modeling efforts. The specific objectives are:

1. Summarize and review the model and previous applications of the LT model
2. Use the LT model to calculate winter precipitation fields of the Juneau Icefield for the period 1979-2013
3. Perform a series of sensitivity experiments varying model parameters, horizontal grid resolution, and the input dataset to assess the robustness of the LT model results
4. Create a winter precipitation index map of the Juneau Icefield that can be utilized in a glacier mass balance model

In contrast to the previous studies, observations to validate the results of the LT model and constrain model parameters are scarce. Nevertheless, we determined that the precipitation pattern derived from the LT model is robust and an improvement from previous methods of precipitation downscaling for the Juneau Icefield region. Based on the results, we also suggest locations for potential precipitation gauges on the icefield that would improve the validation of the LT model results.

1.5 Author Contributions

This thesis will be developed into a manuscript to be submitted to the Journal of Geophysical Research for publication. I, Aurora Roth, am the first author of this publication with Dr. Regine Hock (advisor),

Dr. Thomas Schuler, and Dr. Peter Bieniek as co-authors. Dr. Schuler provided the original code for the LT model and contributed comments and edits to the final manuscript. Dr. Bieniek provided the climate data used to force the LT model, contributed to constructive discussion, and reviewed the manuscript. Dr. Regine Hock assisted with interpretation of the results, provided significant comments and editing of the manuscript, and provided extensive guidance and mentorship in every stage of the process. As first author, I configured the LT model for the Juneau Icefield region, manipulated climate data as needed to use with the LT model, generated all results, conducted the data analysis, and created all figures. I wrote the full draft of manuscript that was later edited by the co-authors.

Chapter 2[1]

2.1 Study Site

The Juneau Icefield is located on the border between Alaska and Canada in the Coast Mountains (Figure 2.1 and covers an area of 4149 km^2 (Kienholz et al., 2015). The icefield ranges in elevation from sea level in the southwest margin, where the town of Juneau is located, to 2400 m a.s.l.. Due to topographic effects, the icefield is divided into a maritime western portion that receives roughly three to four meters of precipitation per year (Pelto et al., 2013) and a significantly drier eastern portion.

The icefield is in the direct path of easterly moving storms that cross the Gulf of Alaska, transporting warm, moist air to southeast Alaska from the Pacific. When these moisture-laden air masses encounter the steep terrain of the Coast Mountains, they are forced to uplift and the moisture cools enough to condense into precipitation. While there are other processes that cause the uplift of air masses and precipitation events, the orographic lifting mechanism is always present and defines the average precipitation pattern of the region. As air masses continue over the mountain divide and descend on the eastern side, they have relatively little moisture available, thus creating the steep precipitation gradient pattern apparent on the Juneau Icefield.

Based on the Randolph Glacier Inventory there are 162 individual glaciers making up the Juneau Icefield (Kienholz et al., 2015). Taku Glacier, Mendenhall Glacier, and Lemon Creek Glacier, in the southwest corner of the icefield, are the most widely studied glaciers of the icefield due to their proximity to Juneau (Figure 2.1). The largest outlet glacier is Taku Glacier, a former tidewater glacier with an area of 735 km^2 and a length of 60 km (Kienholz et al., 2015). Taku Glacier has displayed an interesting advance/retreat pattern in the last centuries, contrasting with regional glacier change trends, and is currently advancing. On the drier eastern side, Llewellyn Glacier is the second largest glacier (450 km^2, 37.5 km long) of the icefield and is one of the largest glaciers in British Columbia. Llewellyn Glacier has been receding rapidly, especially in the past two decades, and has receded the most, in terms of surface area, of all the outlet glaciers in the icefield.

(Ziemen et al., 2016) provide a review of previously reported specific mass balance rates for different time periods ranging from 1948 to 2010 for the entire Juneau Icefield and of Taku Glacier derived by both the geodetic and glaciological methods. There is consensus that the icefield-wide specific mass balance rate was negative during all investigated periods. However, the specific mass balance rate of Taku Glacier was slightly positive during all periods of investigation consistent with its current advance.

[1] To be submitted as Roth, A., R. Hock, T. Schuler, and P. Bieniek (2016). Applying a model of orographic precipitation to improve mass balance modeling of the Juneau Icefield, AK. *Journal of Geophysical Research*

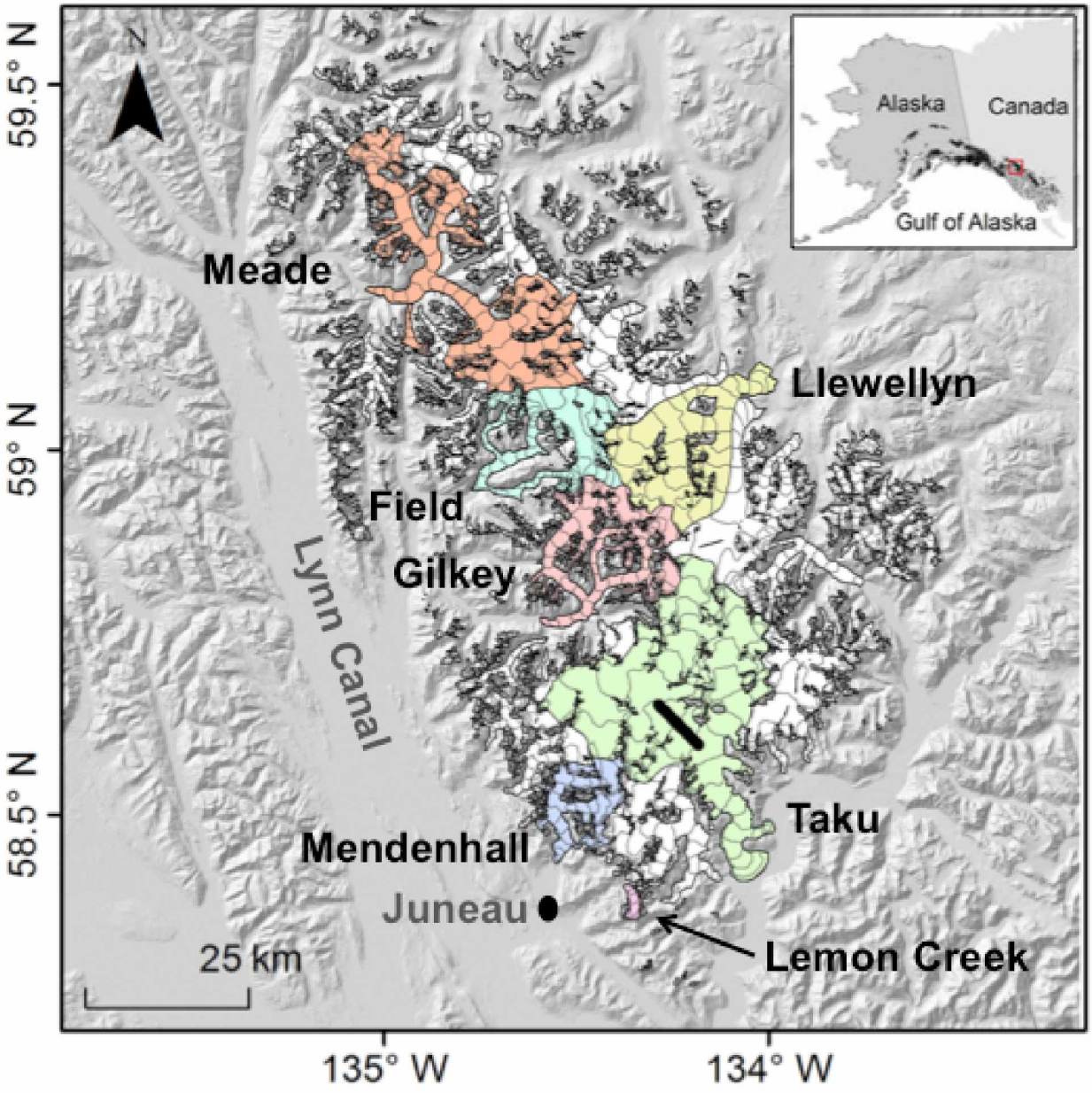

Figure 2.1. Location and topography of the Juneau Icefield. Major outlet glaciers are marked (Lemon Creek, Medenhall, Taku, Gilkey, Llewellyn, Field, and Meade Glaciers), as well as the location of the town of Juneau. The black line on Taku Glacier shows the location of the transect of net accumulation observations taken in 1998, 2004, 2005, 2010, and 2011, (Pelto et al., 2013) used for model validation. Contour lines (grey) within the icefield area show topography at 100 m intervals. The glacier outlines are from Kienholz et al. (2015). The hillshaded topography is the SRTM DEM at 30 m resolution. Inset: The location of the Juneau Icefield (red box) on the Alaska and Canada border and on the coast of the Gulf of Alaska.

2.2 Model Description

2.2.1 The Linear Theory Model

The LT model was first introduced by Smith and Barstad (2004). Variations of the original model have since been used (Table 2.1), but the core equations and concepts have persisted. The following is an overview of the core model, which is addressed in full in Smith and Barstad (2004) with an evaluation of model skill discussed in Barstad and Smith (2005). More recent model variations will be discussed in Section 2.2.2.

Air masses are assumed to be saturated and are driven by winds toward a topographic barrier. An air mass is forced to uplift as it passes over the barrier, which causes condensation of water vapor to cloud water over the windward slope. Cloud water is advected downstream and converted into falling hydrometeors according to a timescale parameter, τ_c. The hydrometeors fall to the surface on a time scale τ_f. Hydrometeors and cloud water continue to be advected downstream with the airflow. As cloud water and hydrometeors descend over the lee side of the topographic barrier, they evaporate or precipitate depending on the atmospheric conditions. Thus, the spatial pattern and intensity of precipitation is determined by (1) the topography over which the air mass is uplifting, (2) microphysical processes that control the rate of condensation and hydrometeor formation and fallout, (3) atmospheric conditions (including temperature, wind speed, water vapor, and stability of the air column), and (4) airflow dynamics (velocity of air masses vertically and horizontally over terrain).

The model treats core aspects of orographic precipitation generation as linear processes despite their well-known nonlinear characteristics. Linear mountain wave theory is used to solve for variations in vertical velocity of air masses with altitude. It assumes that the topographic barrier altitude is relatively small compared to vertical wavelength of mountain waves created by crossing the barrier in a stably stratified atmosphere. The cloud time scales, τ_c and τ_f, are used to represent linear approximations of cloud microphysics processes. These assumptions allow for the investigation of the major processes governing orographic precipitation with relatively simple and compact equations. Furthermore, the LT model requires only a limited number of model inputs and is relatively fast to run depending on spatial resolution and time steps.

The LT model is limited to situations where the atmosphere is stable and where air masses do not experience blocking. The LT model assumes that air masses are saturated, and thus it is only applied when relative humidity exceeds a defined threshold, typically 90% (Crochet et al., 2007; Schuler et al., 2008).

The LT model is based on two steady-state advection equations that describe two groups of atmospheric water, cloud water and hydrometeors, in a horizontal domain described by the coordinates x and y:

$$\frac{Dq_c}{Dt} \approx \mathbf{U}\cdot\nabla q_c = S(x,y) - \frac{q_c(x,y)}{\tau_c}, \tag{2.1}$$

Table 2.1. A summary of the previous glaciological applications of the LT model and this study for a comparison of LT model parameter values. Values for the cloud timescale, τ, and the atmospheric stability (Brunt-Väisälä frequency), N_m, are listed if reported in the reference.

	Crochet et al. (2007)	Jóhannesson et al. (2007)	Schuler et al. (2008)	Jarosch et al. (2012)	Crochet (2012)	This study
Region	Iceland	Iceland	Svartisen Ice Cap, Norway	Western Canada	Iceland	Juneau Icefield, Alaska
Domain size	521 km x 361 km	521 km x 361 km	120 km x 125 km	1000 km^2	521 km x 361 km	156 km x 157 km
Input climate data and resolution	ERA-40, 1.125°	ERA-40, 1.125°	ERA-40, 1.125°	NARR, 32 km	ERA-40, 1.125°	WRF: ~20 km, ERA-Interim: ~0.7°
LT model resolution	1 km	1 km	1 km	1 km	1 km	1 km
Cloud timescale, τ	1200 s	1500s	1200 s	$\tau = \tau_f = \tau_c$ Fall speeds calculated at every time step using Heymsfield (2007). Exp 1: median τ = 1004 ± 578 s Exp 2: median τ = 1178 ± 683 s	τ_f and τ_c calculated separately at every time step. τ_f parameterized in terms of temperature. τ_c calculated by Sinclair (1994)	$\tau = \tau_f = \tau_c$ calculated at every time step. Fall speeds (v_{snow} and v_{rain}) as constant tuning parameters. Ref run: median τ = 1864 ± 683 s
Atmospheric stability (Brunt-Väisälä frequency), N_m	0.004 s^{-1}	0.003 s^{-1}	0.004 s^{-1}	Calculated at every time step following Durran and Klemp (1982) Eq. 3	Calculated at every time step following Durran and Klemp (1982) Eq. 21	Calculated at every time step following Durran and Klemp (1982) Eq. 3 Mean N_m = 0.004 s^{-1}
Calibration data	**(1)** 40 precipitation gauges **(2)** Observed winter mass balances across three ice caps (5-12 yrs temporal coverage)	Same as Crochet et al. (2007)	**(1)** 14 precipitation gauges **(2)** Mean specific winter mass balances of four glaciers for 1970-2002	154 precipitation gauges	Same as Crochet et al. (2007)	Net accumulation along an 8.5 km transect on upper Taku Glacier for five years

$$\frac{Dq_h}{Dt} \approx \mathbf{U}\cdot\nabla q_h = \frac{q_c(x,y)}{\tau_c} - \frac{q_h(x,y)}{\tau_f}, \tag{2.2}$$

where $q_c(x,y)$ and $q_h(x,y)$ are the vertically integrated cloud water density and hydrometeor density respectively, $\mathbf{U} = V\mathbf{x} + U\mathbf{y}$ is the advecting wind vector with northward and eastward components U and V respectively, τ_c is the time required to convert cloud water into hydrometeors, and τ_f is the time required for hydrometeors to reach the ground. These time constants generally range from 200 s to 2000 s (Smith and Barstad, 2004) and their determination will be discussed in Section 2.2.2.2.

$S(x,y)$ is the vertically integrated condensation rate to cloud water as a response to uplift over terrain, referred to as the source term. $S(x,y)$ is a function of the thickness of the ambient moist layer, an uplift sensitivity factor as a function of surface humidity and lapse rate, and the terrain-forced vertical air velocity which is solved for using linear mountain wave theory. These terms are calculated using physical constants and meteorological input data.

Stepping through these foundational steady-state equations we see the amount of cloud water at a given time is determined by the balance of the creation of cloud water through condensation as a response to uplift, $S(x,y)$, and the transformation rate of cloud water to hydrometeors, $\frac{q_c(x,y)}{\tau_c}$. Similarly, the amount of hydrometeors at a given time is determined by the balance of the transformation rate of cloud water to hydrometeors, $\frac{q_c(x,y)}{\tau_c}$, and the loss of hydrometeors due to fallout, $\frac{q_h(x,y)}{\tau_f}$. The final term in Equation (2.2) is then precipitation, $P(x,y)$, where

$$P(x,y) = \frac{q_h(x,y)}{\tau_f}. \tag{2.3}$$

To obtain the general solution for orographic precipitation, Equations (2.1) and (2.2) are first transformed into Fourier space in the horizontal plane (x- and y-directions) for computational efficiency. Following some algebraic manipulation, the Fourier transform of the distributed precipitation rate $\hat{P}(k,l)$ is

$$\hat{P}(k,l) = \frac{\hat{S}(x,y)}{(1+i\sigma\tau_f)(1+i\sigma\tau_c)}, \tag{2.4}$$

where $\hat{S}(k,l)$ is the Fourier transform of the source term, k and l are the horizontal components of the wavenumber, $i = \sqrt{-1}$, and $\sigma = Uk + Vl$ is referred to as the intrinsic frequency.

In this formulation $\hat{S}(k,l)$, is evaluated as

$$\hat{S}(k,l) = \frac{C_w i\sigma\hat{h}(k,l)}{1 - imH_w}, \tag{2.5}$$

where C_w is an uplift sensitivity factor as a function of surface humidity and lapse rate, $\hat{h}(k,l)$ is the Fourier transform of the terrain, H_w is the thickness of the moist layer, and m is the vertical wavenumber. The expression for $\hat{S}(k,l)$ was derived by combining the vertical integral of the condensation rate with linear Boussinesq mountain wave theory. We refer the reader to Equations 10–16 in Smith and Barstad (2004) for a detailed derivation of $\hat{S}(k,l)$.

Variable m controls the depth and tilt of the forced air uplift and is a function of the moist Brunt-Väisälä frequency, N_m, a quantity describing atmospheric stability, such that

$$m = \left[\left(\frac{N_m^2 - \sigma^2}{\sigma^2} \right) (k^2 + l^2) \right]^{\frac{1}{2}}. \tag{2.6}$$

The combination of Equations (2.4) and (2.5) results in a single expression representing the LT model:

$$\hat{P}(k,l) = \frac{C_w i\sigma \hat{h}(k,l)}{(1 - imH_w)(1 + i\sigma\tau_f)(1 + i\sigma\tau_c)} \tag{2.7}$$

Equation (2.7) shows that precipitation pattern and amount depend on terrain ($\hat{h}(k,l)$), the uplift sensitivity factor (C_w), moist layer thickness (H_w), stability of the atmosphere (N_m), wind (σ), and the cloud water and hydrometeor formation timescales (τ_c and τ_f). Terrain is the only gridded variable used in this calculation.

$\hat{P}(k,l)$ is transformed back into the x-y space domain and is added to the large scale background precipitation, P_∞, that accounts for large-scale frontal and convective precipitation separate from orographic precipitation:

$$P(x,y) = \max \left[\iint \hat{P}(k,l) e^{i(kx+yl)} dk dl + P_\infty, 0 \right]. \tag{2.8}$$

P_∞ is calculated by applying Equation (2.7) to the coarse resolution terrain that the input climate data assumes. The solution to this is then subtracted from the coarse climate data precipitation fields, leaving a coarse precipitation field that excludes any orographic effects. Bilinear interpolation is used to distribute P_∞ to the increased resolution grid of $\hat{P}(k,l)$.

Equation (2.7) is formulated such that the solution can be negative. If the sum of the orographic precipitation and background precipitation is negative then the value is set to 0 as shown in Equation (2.8). This represents leeside evaporation in the model as airflow descends.

2.2.2 Tuning Parameters

While the LT model is physically-based, there are several free parameters that must be adjusted and tuned for the model results to match available observations. Early applications of the LT model required the optimization of the parameters N_m, τ_c and τ_f that were assumed constant in time and space (Smith and Barstad, 2004; Barstad and Smith, 2005; Crochet et al., 2007; Jóhannesson et al., 2007; Schuler et al., 2008). Table 2.1 shows how previous studies using the LT model for glaciological applications differed in their values or parameterizations of these variables. Following Jarosch et al. (2012) and Crochet (2012), we implement parameterizations of these variables which utilize physical constants, tuning parameters, and the input climate variables at every time step so that N_m, τ_c, and τ_f vary in time.

2.2.2.1 Atmospheric Stability, N_m

The parameterization and calculation of N_m, the moist Brunt-Väisälä frequency, is not trivial and can be approximated with a variety of methods. The method employed in this model version follows Durran and Klemp (1982), who put forth a new expression of N_m that is both a good approximation compared with previous expressions in the literature and a more simple formulation for practicality in modeling applications. N_m is calculated as a function of temperature and the moist adiabatic lapse rate, Γ_m, where

$$N_m^2 = \frac{g}{T}(\frac{dT}{dz} + \Gamma_m), \tag{2.9}$$

and g is gravitational acceleration, T is temperature of the atmosphere which varies with altitude,z, and the gradient $\frac{dT}{dz}$ is the environmental lapse rate. Γ_m describes how temperature varies with altitude under saturated conditions and is calculated using physical constants in a standard form (Stone and Carlson, 1979)). In summary, N_m is not a tuning parameter as in previous studies, but is instead calculated from the coarse input climate data fields and physical constants allowing the most appropriate value to be used at every time step based on atmospheric conditions. N_m is calculated for every grid cell in the coarse input climate data grid and then the domain averaged value is used in the calculation of orographic precipitation. Barstad and Smith (2005) report that typical values of N_m range between 0 s^{-1}, representing an atmosphere with no stratification, and 0.01 s^{-1} representing a stable stratified atmosphere. The assumptions of the LT model are violated when there is an unstable atmosphere, represented by $N_m < 0$.

2.2.2.2 Cloud Timescale, τ

As in most previous studies (see Table 2.1), we set τ_c and τ_f to the same value where $\tau = \tau_c = \tau_f$. While τ_f can be easily approximated by considering the height at which the hydrometeors are falling, a simple relation for τ_c is more difficult to formulate. There is no direct relationship between τ_c and τ_f, but according to previous authors, the model behavior is most sensitive to the total timescale of both processes, and the difference between these values is less important. For convenience, we will adopt this approach and the timescales will subsequently be referred to as a singular τ.

τ is calculated following the concept of τ_f, the hydrometeor fallout time scale, which is dependent on the height of fallout from the atmospheric moist layer, H_w, and the fall speed of the hydrometeors, v, such that

$$\tau = \overline{\tau_f(x,y)} = \overline{\frac{H_w(x,y)}{v(x,y)}}. \tag{2.10}$$

H_w and v are both gridded quantities at the resolution of the course input climate data. The thickness of the atmospheric moist layer, H_w, is calculated directly from input climate data grids. At each grid cell, the hydrometeor speed, v is a function of temperature with bounding values such that hydrom-

eteors fall more slowly at colder temperatures. The lower bound of hydrometeor fall speed is snow fall speed, v_{snow}, and the upper bound is rain fall speed, v_{rain}. In contrast to other implementations of the LT model, these two values necessary for calculating τ are used as tuning parameters rather than the value of τ itself.

At each time step, the domain average of τ values at each grid cell is calculated. This average value is the quantity of τ used in the calculation of precipitation across the domain in Equation 2.7. Thus, precipitation is calculated with a τ value that is consistent across the domain but varies in time. This is different from previous studies where τ was used as a tuning parameter and was fixed both spatially and in time. Typical values of τ in previous studies are between 200 s and 2000 s (Barstad and Smith, 2005; Crochet et al., 2007; Schuler et al., 2008). Table 2.1 provides a summary and comparison of τ values and methods for calculating τ used here and in previous studies.

2.2.2.3 Hydrometeor Fall Speeds, v_{snow} and v_{rain}

The calculation of the hydrometeor fall speed, v, at each grid cell is a function of the vertically (pressure levels) averaged temperature, $\overline{T}$, at each grid cell where the average is weighted by moisture content at each pressure level. v also relies on v_{snow}, v_{rain}, a transition temperature, T_{mid}, and a transition window σ_T such that

$$v = \begin{cases} v_{\text{snow}}, & \overline{T} < T_{mid} - \frac{\sigma_T}{2}, \\ \frac{1}{\sigma_T}\left(\overline{t} - T_{mid} - \frac{\sigma_T}{2}\right)(v_{\text{rain}} - v_{\text{snow}}) + v_{\text{rain}}, & T_{mid} - \frac{\sigma_T}{2} \leq \overline{T} \leq T_{mid} + \frac{\sigma_T}{2}, \\ v_{\text{rain}}, & \overline{T} > T_{mid} + \frac{\sigma_T}{2}. \end{cases} \tag{2.11}$$

T_{mid} is generally between -1°C and 1°C. For values of $\overline{T}$ inside the bounds of $T_{mid} \pm \frac{\sigma_T}{2}$, a linear transition between the bounding values of v_{snow} and v_{rain} is calculated and fitted to the width of the transition window, σ_T . σ_T is generally accepted to range from $\pm 2^{\circ}C$ to $\pm 6^{\circ}C$ centered about T_{mid}. In this study, we used $T_{mid} = 0^{\circ}C$ and $\sigma_T = 4^{\circ}C$.

While the expression and general concept of τ_f is the same for all studies which calculate, rather than tune, τ, recent studies have used different parameterizations of the fall speeds, v, in their calculation of τ (Table 2.1. Jarosch et al. (2012) fully parameterized the hydrometeor fall speed in terms of physical constants and input climate data based on Heymsfield (2007). Crochet (2012) calculated hydrometeor fall speeds as a function of atmospheric mixing ratios derived from the input climate data and a free parameter whose value was determined from Sinclair (1994). However, Crochet (2012) showed that further parameterization and increased model complexity did not significantly improve or alter LT model results.

We tune the parameters v_{snow} and v_{rain} and perform a sensitivity analysis to evaluate the impact of the choice of v_{snow} and v_{rain} on the calculated τ values and the results of the LT model. Average

snow fall speed is generally accepted to be 1.0 m s^{-1} for dry snow and 2.0 m s^{-1} for wet snow based on empirical evidence (Yuter et al., 2006; Locatelli and Hobbs, 1974). Rain fall speeds can range from less than 2.0 m s^{-1} to 9.0 m s^{-1}, but Yuter et al. (2006) show that during a specific rain event hydrometeors exhibited a fall speed of 4.0 m s^{-1} most often.

2.3 Data and Methods

2.3.1 Digital Elevation Models (DEMs)

The LT model is applied to a digital elevation model (DEM) of 1 km resolution (Figure 2.2). This DEM was bilinearly interpolated from a 30 m resolution DEM from the Shuttle Radar Topography Mission (SRTM) flown over the region in 2000. The 1 km resolution captures the complex features relevant to the physics of the LT model, but it does smooth the terrain. The maximum elevation of the 1 km resolution DEM is 2300 m a.s.l. and the highest peak in the Juneau Icefield region is 2500 m a.s.l..

In this study, we use global scale climate data from ERA-Interim Reanalysis and regional scale climate data from the Weather Research and Forecasting (WRF) model. The assumed topographies associated with both datasets are drastically smoothed due to the coarse resolution. The ERA-Interim topography for the model domain, with ~100 km resolution for global climate applications, is depicted as a smooth ramp with maximum elevation of 1150 m a.s.l.. The model domain is represented by only eight grid points in the ERA-Interim dataset. The WRF topography for the model domain, with ~20 km resolution, depicts a smooth increase and decrease in elevation with a maximum elevation of 1600 m a.s.l and is represented by 70 grid points. Figure 2.2 d-f shows the comparison between the ERA-Interim and WRF topographies and the SRTM DEM.

2.3.2 Meteorological Variables

The meteorological variables used as input in the LT model are air temperature, relative humidity, and wind speed vectors. These data were derived from vertical profiles of ERA-Interim Reanalysis variables dynamically downscaled using the regional atmospheric model of Weather Research and Forecasting (WRF; Skamarock et al., 2008). ERA-Interim Reanalysis climate data are the latest global gridded climate data from ECMWF and extend from 1979 to the present at a spatial resolution of approximately 80 km (Dee et al., 2011). The dataset includes the characterization of the vertical structure of the atmosphere by discretizing the atmosphere into 60 layers that follow constant pressure (pressure levels). WRF was used to downscale the ERA-Interim dataset to a ~20 km grid for Alaska and is currently the best available climate data for Alaska for the recent past (Bieniek et al., 2016). This downscaled dataset will be referred to as the WRF data. Note that this is different from the climate input used by Ziemen et al. (2016) who used WRF to downscale output from a free-running global climate model rather than a reanalysis.

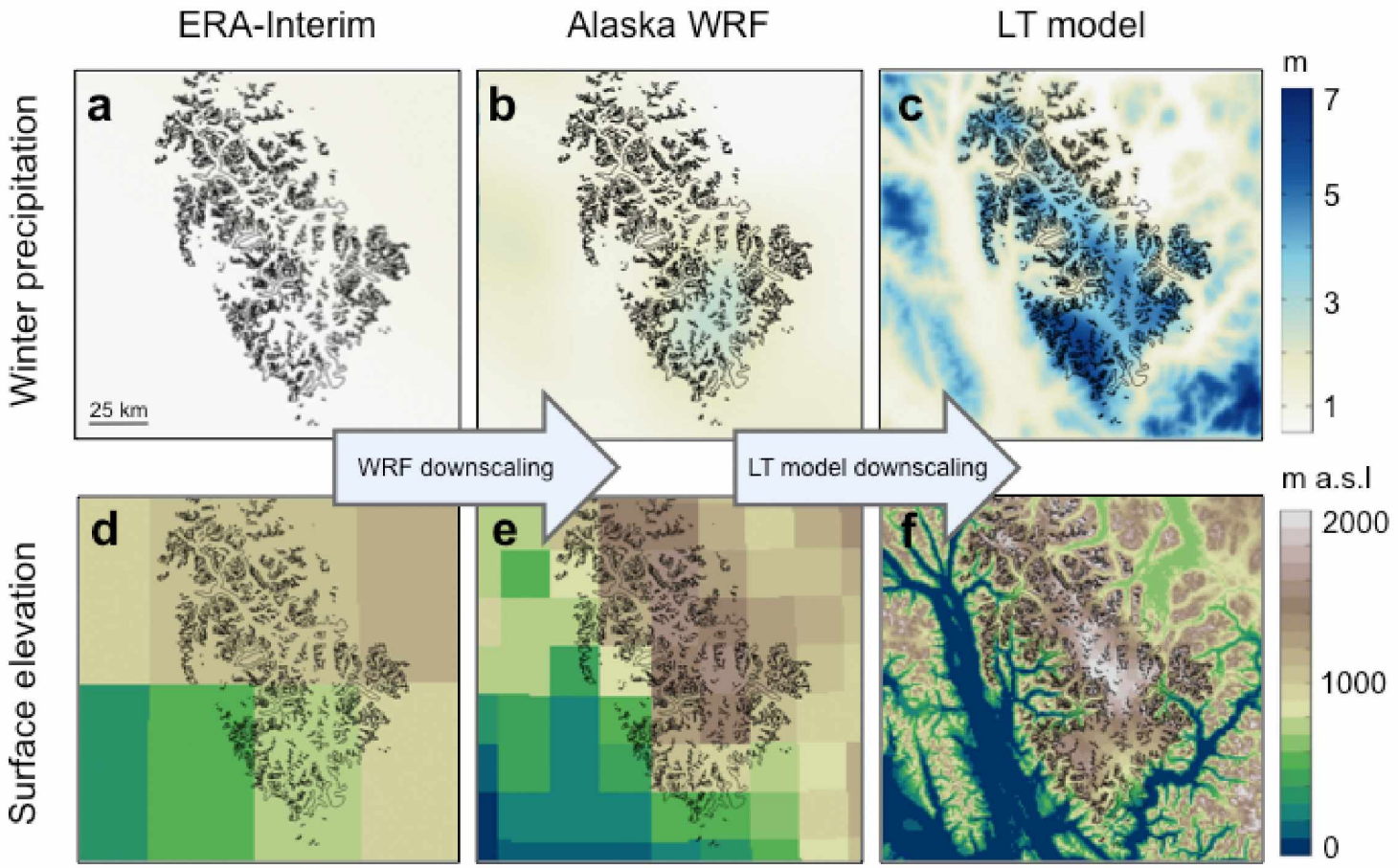

Figure 2.2. Average winter precipitation (1979-2013) and digital elevation models (DEMs) for ERA-Interim, WRF, and LT model. The top row shows average winter precipitation (1979-2013) for (a) ERA-Interim (Dee et al., 2011), (b) WRF (Bieniek et al., 2016), (c) and the reference run results of the LT model. For comparison to the LT model results, the average winter precipitation grids for ERA-Interim (a) and WRF (b) have been interpolated to 1 km resolution from their original resolutions. The bottom row (d–f) shows the DEM used for each dataset with the original resolutions. The resolution of the ERA-Interim DEM (d) is ~100 km and WRF DEM (e) resolution is ~20 km. The DEM used for the LT model (f) is the SRTM DEM with 1 km resolution. The arrows indicate the increasing resolution of the downscaling by WRF and then the LT model. In each grid, the outline of the Juneau Icefield is shown in black (Kienholz et al., 2015).

The meteorological variables were obtained on hourly time steps, but the LT model was run on 6-hour time steps. The instantaneous values of each variable at 0:00, 6:00, 12:00, and 18:00 hours for each day were used. Variables were obtained for four different pressure levels (1000, 900, 800, 750 hPa) that span an altitude range from sea level to roughly 3000 m a.s.l.. At each pressure level, specific humidity was converted to relative humidity following standard calculations. For every 6-hour time step, the gridded fields were vertically integrated and horizontally averaged over the domain and used to calculate the quantities needed in Equation 2.7.

2.3.3 Background Precipitation, P_∞

Hourly precipitation data from WRF were summed resulting in precipitation fields for every 6-hour time step. These data were used to calculate the background precipitation that is unrelated to orographic effects, P_∞ in Equation 2.8. The WRF precipitation data includes some minor orographic enhancement from the assumed WRF topography that has to be removed prior to applying the LT model to the finer resolution DEM to avoid double-counting of the orographic effect.

To do so the LT model is applied to the coarse WRF topography using the WRF meteorological variables. The resulting orographic precipitation is then subtracted from the WRF precipitation data, resulting in the so-called background precipitation field, P_∞. The background precipitation field, interpolated to the finer resolution grid, is then added to the orographic precipitation calculated on the finer resolution grid (Equation 2.8).

2.3.4 Glacier Mass Balance Data

Previous studies have calibrated the free parameters of the LT model by matching model results with precipitation gauge measurements and glaciological measurements. While precipitation gauges have uncertainties and errors associated with them, this is the preferred first order method because there is a direct comparison of the same variable between the model and observations. However, there are no precipitation gauge data available for the Juneau Icefield.

Glaciological data must then be used to calibrate the LT model parameters. Winter season mass balance measurements have been used in previous studies because these data capture snow accumulation and the effect of melt tends to be small. Compared to the data available to previous studies, there is a lack of strictly winter season mass balance data for the Juneau Icefield.

The Juneau Icefield Research Program (JIRP) has created an extensive annual specific mass balance data set for Taku and Lemon Creek Glaciers. These records are the longest continuous glacier annual mass balance data sets in North America. However, these data are reported as area-averaged specific mass balances so the spatial pattern of the LT model results cannot be validated. The raw point measurements from the 22 snow pits used to calculate these area-averaged annual specific mass balances

are not publicly available.

For five years, JIRP conducted probing transects in the accumulation area to better determine the distribution of net accumulation. We compared the LT model results to these net accumulation measurements as these data are reported as point measurements with their specific location and elevation by Pelto et al. (2013). These data were collected along a transect of 60 points on Taku Glacier in late July of 1998, 2004, 2005, 2010, and 2011 by probing to the last summer surface at horizontal intervals of 200 m. The transect was positioned just above the transient snow line and ranged from 900 m a.s.l. to 1150 m a.s.l. (Figure 2.1). Three point measurements made within 25 m were averaged to determine the snowpack depth at each probing location. These data were converted to water equivalent using mean snow density observed in snow pits along the transect in three locations (Pelto et al., 2013).

These net snow accumulation observations cannot be directly compared to the output of the LT model, total precipitation. First, some of the precipitation falls as rain. Second, the observations include mass loss due to melt, sublimation or redistribution of snow by wind. In particular, we expect that significant melt has occurred by the time the snow accumulation measurements were performed in summer well after the start of the melt season (Figure 2.3).

To allow direct comparison between model results and observations, we compute net snow accumulation from the modeled precipitation by first extracting the snow portion of precipitation and then applying a standard temperature-index model to account for melt. Other ablation processes are considered to be negligible. The snow portion of precipitation is calculated using the model scheme that differentiates between the fall speeds of snow and rain (Equation 2.11). The vertically average temperature, $\overline{T}$, calculated as a weighted average based on the moisture content at each grid cell in the model domain is used to determine whether hydrometeors in a grid cell fall with a speed of v_{snow} or v_{rain}. The precipitation is recorded as only snow or only rain in these grid cells. If $\overline{T}$ is within the transition window around T_{mid} so that the fall speed is between v_{snow} and v_{rain}, then a similar linear transition scheme as in Equation 2.11 is used to calculate the fraction of snow of the total precipitation in the grid cell.

We apply a standard temperature-index melt model to account for melt during the time period of each observation. Near surface air temperature is downscaled from the native climate data resolution to the LT model resolution following Machguth et al. (2009) using the international standard atmosphere lapse rate Γ = -0.0065 K m^{-1}. Melt, M, is calculated at every 6 hour time step by multiplying the downscaled near surface air temperature,T, by a melt factor, f_m, as follows:

$$M = \begin{cases} f_m(T - T_0), & T > T_0 \\ 0, & T \leq T_0 \end{cases} \tag{2.12}$$

The melt threshold temperature, T_0, was set at 0°C and a range of melt factors for snow were applied whose values were based on Braithwaite (2008). He summarizes and reports mean snow

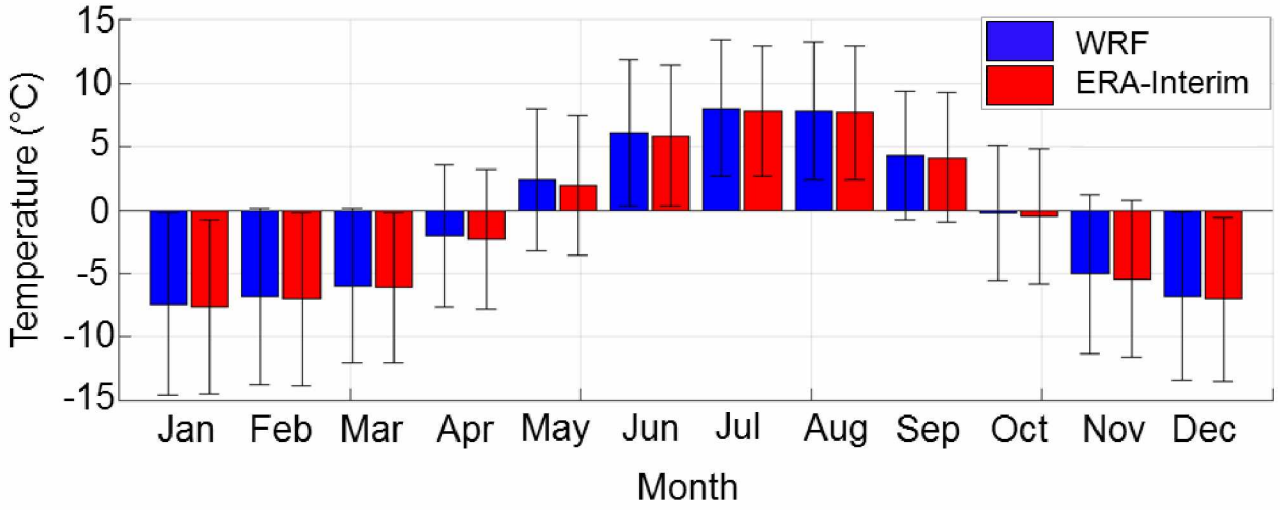

Figure 2.3. Monthly mean temperatures over the Juneau Icefield from WRF (blue) and ERA-Interim (red) from 1979-2013. For both datasets, the temperature grids at every time step were vertically and horizontally averaged. Vertical averaging was done over the four pressure levels used. Horizontal averaging was applied over the entire domain. The mean temperature of each month in the 1979-2013 model period was calculated. The error bars represent the standard deviation about the mean monthly temperature.

degree-day factors used in previous studies with 95% confidence intervals that range between 3.2 mm d^{-1} K^{-1} and 6.2 mm d^{-1} K^{-1} for all studies and suggests that 4.1 ± 1.5 mm d^{-1} K^{-1} be used as a first-assumption degree-day factor for snow melt around the equilibrium line altitude (ELA) for an unknown glacier. This closely matches the degree-day factor of 4.0 mm d^{-1} K^{-1} for snow used in Ziemen et al. (2016).

Net accumulation was calculated from the LT model results in the grid cells of the model domain that corresponded to the location of the available observations. Initially, we use melt factor of f_m = 4.1 mm d^{-1} K^{-1}, with the units converted to match the 6 hour time steps used in this study. It should be noted that applying the temperature-index model using 6 hour time steps and four different temperature values per day will result in a greater amount of melt calculated per day compared to using daily time steps and daily mean temperatures, as is standard. We used 6 hour time steps in this study to capture precipitation events generated at sub-daily time scales.

Since the glaciological data refer to an unknown start date (stratigraphic time system) we extract net accumulation from the model for the period between 1 October of the previous year and the observation date of each year. Additionally, we assume that all melt water and rain water exits the snow or firn pack and is not retained.

2.4 Model Application and Validation

2.4.1 LT Model Application

The model is set up on an UTM Zone 8 grid at an initial resolution of 1 km with a domain of 156 km x 157 km. The domain was chosen to match the domain used by Ziemen et al. (2016). Bilinear interpolation was used to interpolate the WRF climate grids in Polar Stereographic projection and the SRTM DEM in Alaska Albers Equal Area Projection to the model grid for input. The model was run using 6 hour time steps starting in January 1979 and ending in December 2013. Initial tuning parameters with the following values were used: v_{snow} = 1.0 m s^{-1}, v_{rain} = 4.0 m s^{-1}, T_{mid} = 0°C, and σ_T = ±4°C. This parameter set is considered the reference run. We start with v_{snow} = 1.0 m s^{-1}, the average fall speed of dry snow (Yuter et al., 2006). We start with a rain fall speed value of v_{rain} = 4.0 m s^{-1} as this was the most observed rain fall speed by Yuter et al. (2006) (see Section 2.2.2.3).

The LT model is only applied at a time step if the relative humidity criteria are met. Forcing the model with meteorological variables from the WRF dataset results in 86% of the time steps applying the LT model. Within the time steps where the LT model is run, the atmosphere must be stable for the LT model equations to be valid. If a negative atmospheric lapse rate is calculated from the temperature data at the pressure levels, then the stability, N_m is bounded at 0 so that it cannot be negative, but the LT model is still run. N_m = 0 for 15% of the time steps when the model is forced by WRF.

2.4.2 Model Validation

We compared net accumulation calculated from the results of the LT model reference run to the available glaciological point measurements. Figure 2.4 shows that net accumulation is overestimated by the model for the years 1998 and 2010 and underestimated by the model for 2004, 2005, and 2011. The model best matches observations from 2011. The magnitude of positive and negative bias of the model results is similar with the mean absolute error (MAE) for all years being 0.45 m w.e. (water equivalent). For some values of modeled net accumulation there are multiple corresponding values of observed net accumulation for each year because a subset of locations are contained within individual 1 km grid cells of the model domain.

We calculated the average net accumulation of the observations and model results for the 20 points that had measurements available for all five years. While the model results and observations are weakly correlated when considering all data points (r^2 = 0.35 and MAE = 0.45 m w.e.), there is a much stronger correlation and a substantially smaller MAE for the averaged values (r^2 = 0.89 and and MAE = 0.05 m w.e.). This shows that net accumulation calculated from the LT model results simulates the average pattern of observed net accumulation along the transect, but the amount of net accumulation along the transect for each individual year is over or underestimated by the model.

Figure 2.5 shows that the temperature-index model generates substantial melt during the observation period. Total snow accumulation is reduced by approximately 3.5 m w.e when applying a melt factor of f_m = 4.1 mm d^{-1} K^{-1} to calculate net accumulation. This indicates that melt is a dominant process in this location before the time observations were made in late July, and hence the choice of melt factor can significantly change the modeled net accumulation. To address this uncertainty we also calculated net accumulation from the LT model results using f_m = 3.2 mm d^{-1} K^{-1} and f_m = 6.2 mm d^{-1} K^{-1} based on the range suggested by Braithwaite (2008). Resulting modeled net accumulation along the transect varies by approximately 2 m w.e (Figure 2.5) suggesting that agreement between the model and observations could be improved by varying the melt factor within reasonable limits.

However, we cannot differentiate whether the disagreement between the model results and observations is due to errors in the melt estimation or errors in the amount of precipitation modeled by the LT model and derived snow accumulation. Hence, we refrain from optimizing the melt factor, but the overall good agreement between model results and observations using Braithwaite's (2008) suggested snow melt factor f_m = 4.1 mm d^{-1} K^{-1} is encouraging (Figure 2.4). To evaluate the robustness of results to the choice of LT model parameters we perform a detailed sensitivity analysis (Section 2.6).

2.5 LT Model Results

The precipitation results of the LT model with reference run parameters are shown in Figure 2.2. WRF and ERA-Interim precipitation data are shown for comparison. We assess the amount and pattern of

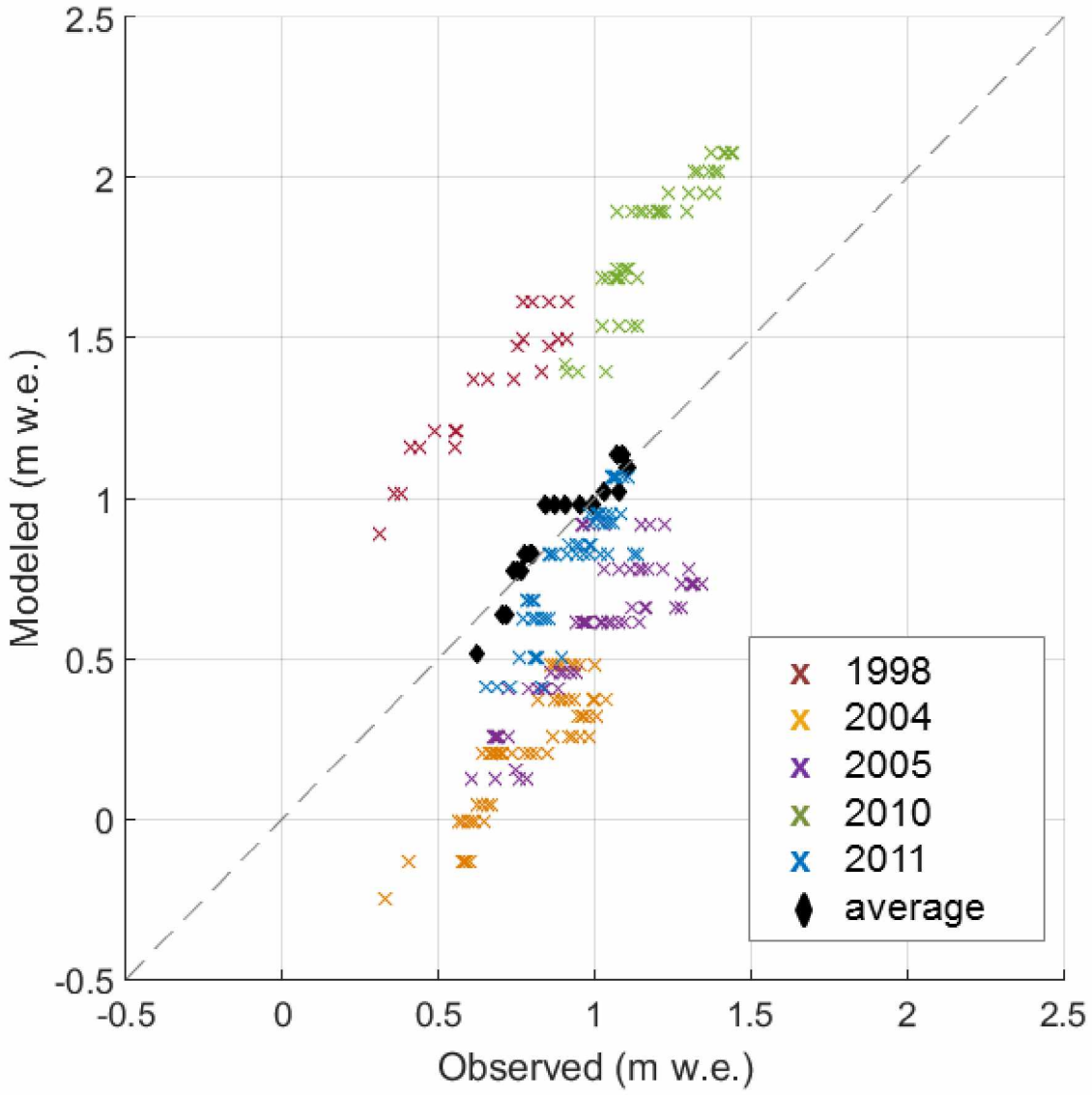

Figure 2.4. Modeled versus observed net accumulation for the individual years 1998, 2004, 2005, 2010, 2011 (colored crosses) and the arithmetic average of these five years (black diamonds). For all data points shown (excluding the average values), $r^2 = 0.35$ and MAE = 0.45 m w.e.. Considering only average values $r^2 = 0.89$ and MAE = 0.05 m w.e.. All observations were made along the same transect, but each year has a different number of observations. Averages were calculated for observation locations with measurements for all five years (20 points). Modeled net accumulation was calculated assuming a start date of 1 October from the previous year of the observation year and the exact date the observations were taken in late July was matched by the model for each year. The model resolution is 1 km so some model grid cells match the location of multiple observation locations. The dashed grey line represents perfect agreement between the observations and model results.

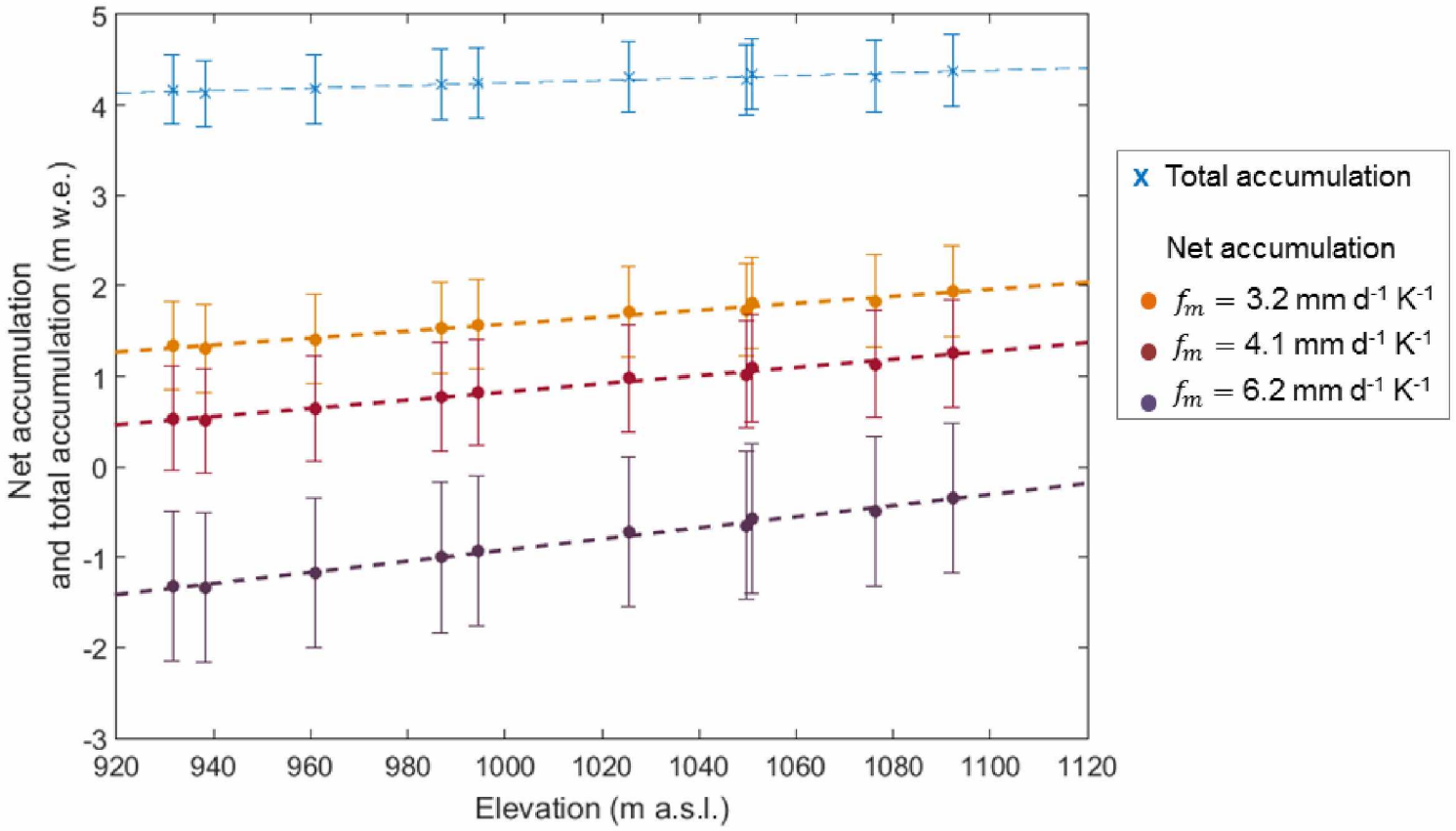

Figure 2.5. Average modeled net accumulation for different melt factors and total accumulation versus elevation. Average modeled net accumulation (i.e. the balance between total snow accumulation and ablation) is expressed in meters water equivalent (m w.e.) for the five observation years versus elevation (m a.s.l.) for grid cells in the model domain that match observation locations. Net accumulation was calculated from 1 October of the previous year to the exact date the observations were made in late July using a temperature-index model to account for melt. The error bars show the standard deviation of the average modeled net accumulation at each location. We calculated net accumulation with three different melt factors. The range of melt factors used here are the minimum and maximum 95% confidence interval of the mean snow degree-day factors used in previous studies investigated by Braithwaite (2008). We used Braithwaite's (2008) suggested snow melt factor of f_m = 4.1 mm d^{-1} K^{-1} for the LT model reference run (red dots). Additionally, average modeled total snow accumulation (blue crosses) is shown to demonstrate the significance of melting for the time period of the observations.

the average total winter precipitation for the entire model period (1979–2013) with the winter season being defined as October–March. The winter season was considered because accurate representation of winter precipitation and resulting accumulation is necessary for mass balance modeling investigations.

The results of the LT model are encouraging and clearly show the expected orographic precipitation pattern lacking in the coarse precipitation fields of the ERA-Interim and WRF datasets. The pattern is more complex than the manually adjusted precipitation field used Ziemen et al. (2016) where precipitation amount increased linearly from West to East on the windward side of the icefield divide and then decreased linearly on the leeward side of the icefield divide. The LT model results show two areas of maximum precipitation corresponding to topographic maxima that surround a local precipitation minimum in the upper area of Taku Glacier on the windward side of the icefield. While a large scale orographic precipitation pattern across the icefield divide is shown, the LT model solution reveals smaller scale effects and heterogeneity of precipitation amounts in response to local topographic maxima. The icefield-wide spatial mean (excluding non-glaciated areas of the domain) of average winter precipitation for the reference run was 3.7 ± 1.1 m and the maximum value of average winter precipitation is 6.3 m located in the southwestern branch of upper Taku Glacier.

The median τ value for the 1979-2013 time period was 1864 ± 683 s. Figure 2.6 shows that the value τ has a seasonal pattern. τ values for every 6 hour time step where the LT model was applied for January 2012 - December 2013 are shown alongside the distribution of τ values for the entire model period (1979-2013) in Figure 2.6. In winter, the lower bound of fall speeds, v_{snow}, is used to calculate τ more often resulting in larger τ values for all winter months (October - March). Conversely, in summer, the upper bound of fall speeds is used to calculate τ more often resulting in smaller τ values. The τ value used in the LT model is a spatial mean over the model domain and Figure 2.6a shows the standard deviation of this spatial mean. Summer τ values have much smaller standard deviations and the mean values show less variability in time compared to winter τ values. This is due to more homogenous fall speeds across the model domain in summer.

2.6 Sensitivity Analysis

We evaluated the robustness of the LT model results by conducting a series of sensitivity experiments. We varied the LT model parameters of snow fall speed (v_{snow}) and rain fall speed (v_{rain}), as well as the horizontal resolution of the underlying DEM, and the climate input data. For each parameter combination, we calculated the icefield-wide spatial mean of the average winter precipitation over the 1979-2013 time period to assess the sensitivity of the amount of average winter precipitation. To assess the sensitivity of the precipitation pattern, we computed the average winter precipitation index defined as the percentage of the local average winter precipitation value at each grid cell to the

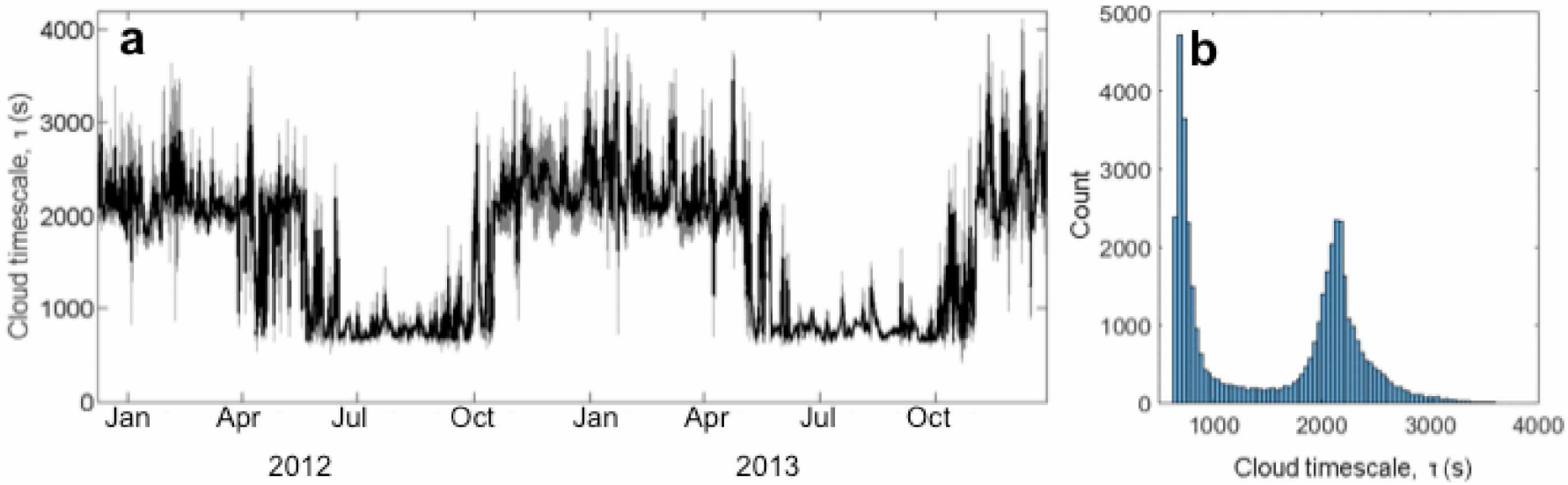

Figure 2.6. Time series of τ values for January 2012 - December 2013 and a distribution of τ values for 1979-2013. (a) A time series of τ values for every 6 hour time step the LT model was applied for January 2012 - December 2013 (black line). These τ values are from the reference run of the LT model. τ values used in the calculation of precipitation represent a spatial mean of variable τ values in every grid cell of the model domain. The grey area represents the standard deviation of this spatial mean at every time step. (b) The distribution of τ values at every 6 hour time step for the entire model period (1979-2013) for the LT model reference run.

icefield-wide spatial mean of average winter precipitation. Values larger than 100% indicate average winter precipitation larger than the spatial mean and vice versa. v_{snow} and v_{rain} are used to calculate hydrometeor fall speed which is used to calculate transient τ values. As τ is a common parameter among all studies that have employed the LT model, we calculated the median τ value for the model time period with the associated median absolute deviation for each parameter combination. We ran the LT model for each parameter combination using a 1 km and 5 km resolution DEM to assess the sensitivity of the LT model to the horizontal resolution of the underlying DEM . Finally, we forced LT model with global scale ERA-Interim meteorological variables directly to explore the necessity of using the computationally expensive regional scale WRF dataset.

It should be noted that other LT model parameters exist which are held constant and not explored in this sensitivity analysis. For all sensitivity experiments $T_{mid} = 0^{\circ}C$ and $\sigma_T = 4^{\circ}C$. Additionally, the choice of domain size and the regions included in the domain influence the LT model results because the domain averaged meteorological input variables and domain averaged τ value are ultimately used to calculate precipitation.

2.6.1 v_{snow}, v_{rain}, and τ

We focused on these parameters because they are unique to the parameterization of the LT model used in this study. Holding all other model parameters constant, we ran the LT model for all parameter combinations from a range of values of v_{snow} and v_{rain}. Reasonable ranges of v_{snow} and v_{rain} were determined from Yuter et al. (2006) where v_{snow} values ranged from 0.2-2.0 m s^{-1} and v_{rain} values ranged from 3.0-5.0 m s^{-1}, using a step size of 0.2 m s^{-1} to traverse each parameter range.

In general, higher fall speeds lead to greater amounts of precipitation with a stronger precipitation gradient because the hydrometeors fall to the ground faster than they are advected across the icefield. With lower fall speeds, the hydrometeors are advected across the icefield more as they fall from the moist layer causing a decrease in precipitation amount and a weaker precipitation gradient across the icefield. Figure 2.7 shows the relationship between v_{snow} and icefield-wide spatial mean of average winter precipitation. For all parameter combinations, the spatial mean of average winter precipitation ranges from 2.5 m to 6.5 m and is positively related to both v_{snow} and v_{rain}. For ranges of the parameters tested here, the precipitation amount is more sensitive to v_{snow} than v_{rain}. A 2.0 m s^{-1} increase of v_{rain} from 3.0 m s^{-1} to 5.0 m s^{-1} causes approximately 0.25 m increase to the spatial mean of average winter precipitation. A similarly sized increase of v_{snow} from 0.2 m s^{-1} to 2.0 m s^{-1} causes an approximately 2.0 m increase to the area averaged mean winter precipitation.

Figure 2.8 shows the average winter precipitation pattern expressed by computing the precipitation index across the icefield for a representative sample of parameter combinations. With increasing v_{snow} and v_{rain} values, the precipitation index increases meaning that the average winter precipitation

values become increasingly larger than the spatial mean, but the areas of high precipitation index occur in the same location for each parameter combination. This indicates that the precipitation pattern is relatively insensitive to the choice of v_{snow} and v_{rain} compared to the sensitivity of the amount of precipitation.

The median τ value calculated for the 1979-2013 time period as a function of v_{snow} is shown in Figure 2.7. τ decreases exponentially as the value of v_{snow} increases and the average winter precipitation increases. This agrees with previous LT model sensitivity experiments of Smith and Barstad (2004) and Barstad and Smith (2005) where longer values of τ resulted in decreased orographic enhancement.

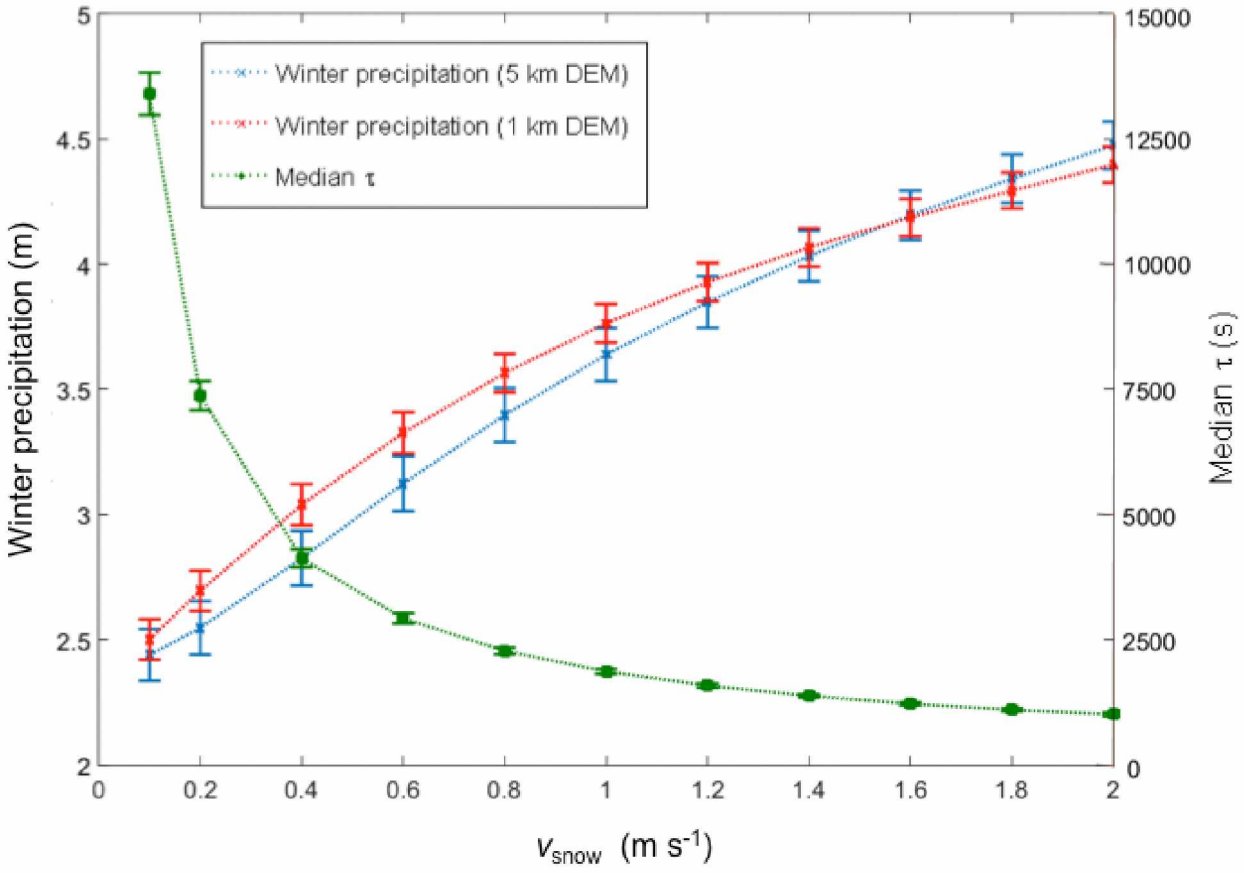

Figure 2.7. Winter precipitation (m) and cloud timescale, τ (s) as a function of snow fall speed, v_{snow} (m s^{-1}). Winter precipitation is the icefield-wide spatial mean of average winter precipitation for the 1979-2013 time period. The results of the two DEM resolutions used in the sensitivity experiments are shown: the 5 km DEM (blue) and the 1 km DEM (red). The median τ value of every time step where the LT model was applied for the 1979-2013 period as a function of v_{snow} is shown by the green curve. Note that τ does not vary with LT model resolution as it is calculated from the meteorological input data and parameters. A rain fall speed of v_{rain} = 4.0 m s^{-1} was used for the data points of each winter precipitation curve (crosses) and the median τ values curve (green squares). For all three curves, the error bars represent the variation of results due to minimum and maximum v_{rain} used. The lower error bars correspond to v_{rain} = 3.0 m s^{-1} and the upper bars correspond to v_{rain} = 5.0 m s^{-1}.

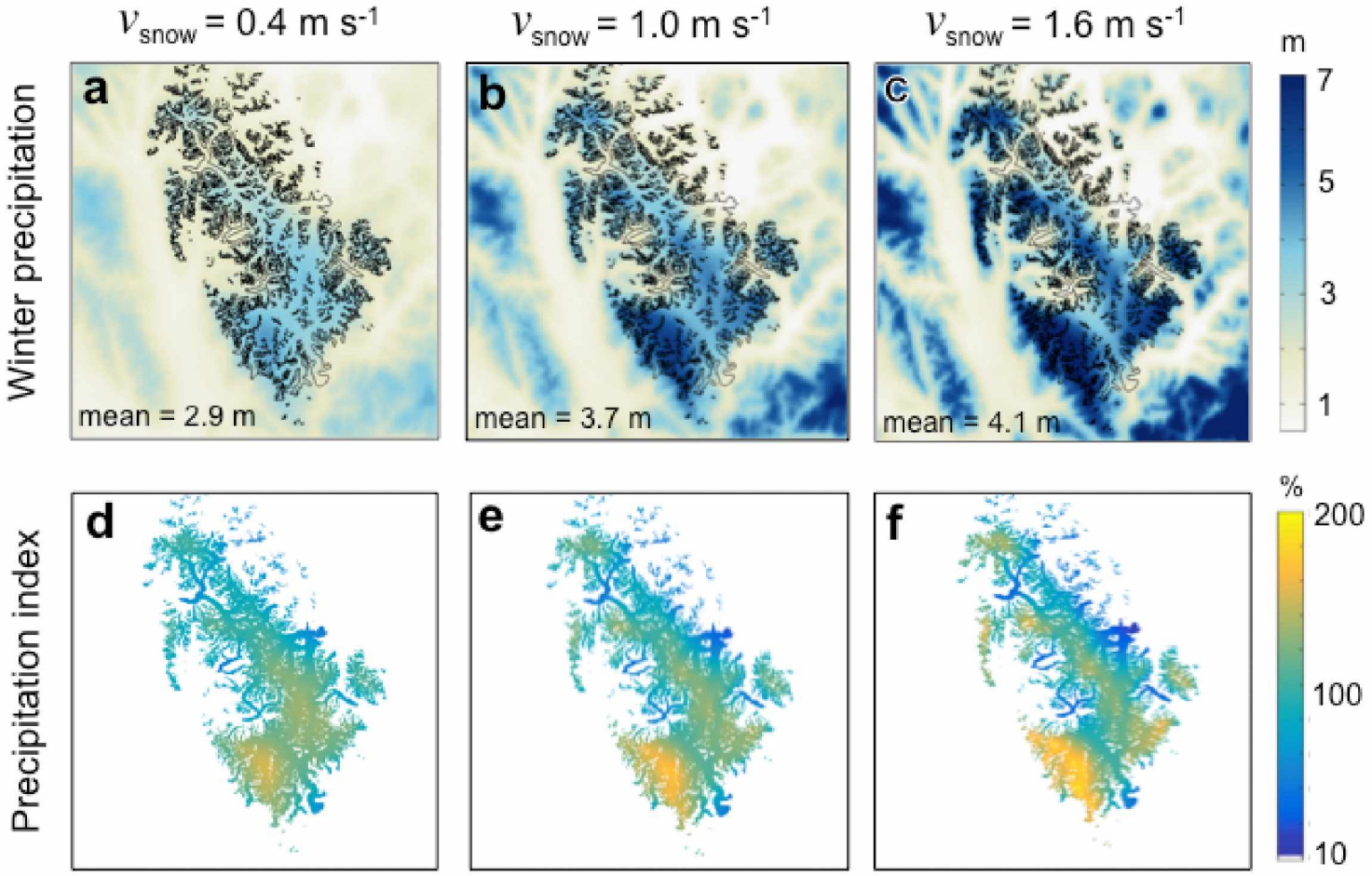

Figure 2.8. Average winter precipitation and precipitation pattern for three v_{snow} values. Modeled average winter (October–March) precipitation (a–c) and precipitation index (d–f) averaged over the time period 1979–2013 for three different values of v_{snow}: v_{snow} = 0.4 m s^{-1}, v_{snow} = 1.0 m s^{-1}, and v_{snow} = 1.6 m s^{-1}. The precipitation index values indicate local deviations from the spatial mean and are computed as the ratio of each grid cell's winter precipitation to the icefield-wide spatial mean of winter precipitation, expressed as a percentage. The means noted in (a–c) refer to the icefield-wide spatial mean.

2.6.2 Horizontal Resolution

The precipitation amount and pattern are also sensitive to the spatial resolution of the DEM used for downscaling with the LT model. This has been explored extensively by previous authors, a summary of which is provided by Crochet et al. (2007). Depending on the model used and the observations available to tune the model, previous studies have chosen DEMs with spatial resolutions between 1 km and 5 km (Crochet et al., 2007). As the resolution decreases, the topography is smoothed and maximum elevations for the region are decreased. As a result, the model calculates less precipitation because air masses experience less uplift within the model.

We compared the variation in model results introduced by the spatial resolution to the variation introduced by the v_{snow} and v_{rain} parameter choices by applying the LT model to a 1 km and 5 km resolution DEM for each parameter combination. Both DEMs were bilinearly interpolated from a 30 m resolution DEM from the Shuttle Radar Topography Mission (SRTM) flown over the region in 2000.

The icefield-wide spatial mean of average winter precipitation for each v_{snow} value is shown for two different DEM resolutions in Figure 2.7. As described previously, the decreased resolution leads to a decrease in precipitation amount. The difference between the spatial mean of the average winter precipitation amount of the two resolutions is at most 0.3 m for $v_{\text{snow}} = 0.4$ m s^{-1}. Similar mean winter precipitation values over the icefield can be calculated with different combinations of DEM resolution and v_{snow} value. Figure 2.9 shows the precipitation pattern expressed with precipitation index values for the LT model reference parameter set applied to each resolution. The pattern of precipitation is similar between the two resolutions despite the slight difference in the icefield-wide spatial mean precipitation amount.

2.6.3 Applying the LT Model to ERA-I Reanalysis

While the downscaled regional WRF dataset is the best available climate dataset for Alaska, it is computationally expensive to produce. For possible future mass balance modeling efforts in Alaska, it may be more effective to directly force the LT model with a readily available global climate data product. We compared the results of the LT model forced by the WRF data (~20 km resolution) and by global scale ERA-Interim climate data (~100 km resolution) to address the necessity of the computationally expensive WRF data in the capability of the LT model to improve mass balance modeling. With this forcing, the DEM used to derive the ERA-Interim data was used to calculate background precipitation and the same meteorological variables previously described were used as input. The fine resolution SRTM DEM was used at 1 km resolution. The reference run parameters of the LT model were used in both instances.

Our results show the ERA-Interim input to the LT model produces an LT model solution with a decreased amount of average winter precipitation compared to the solution produced by the WRF

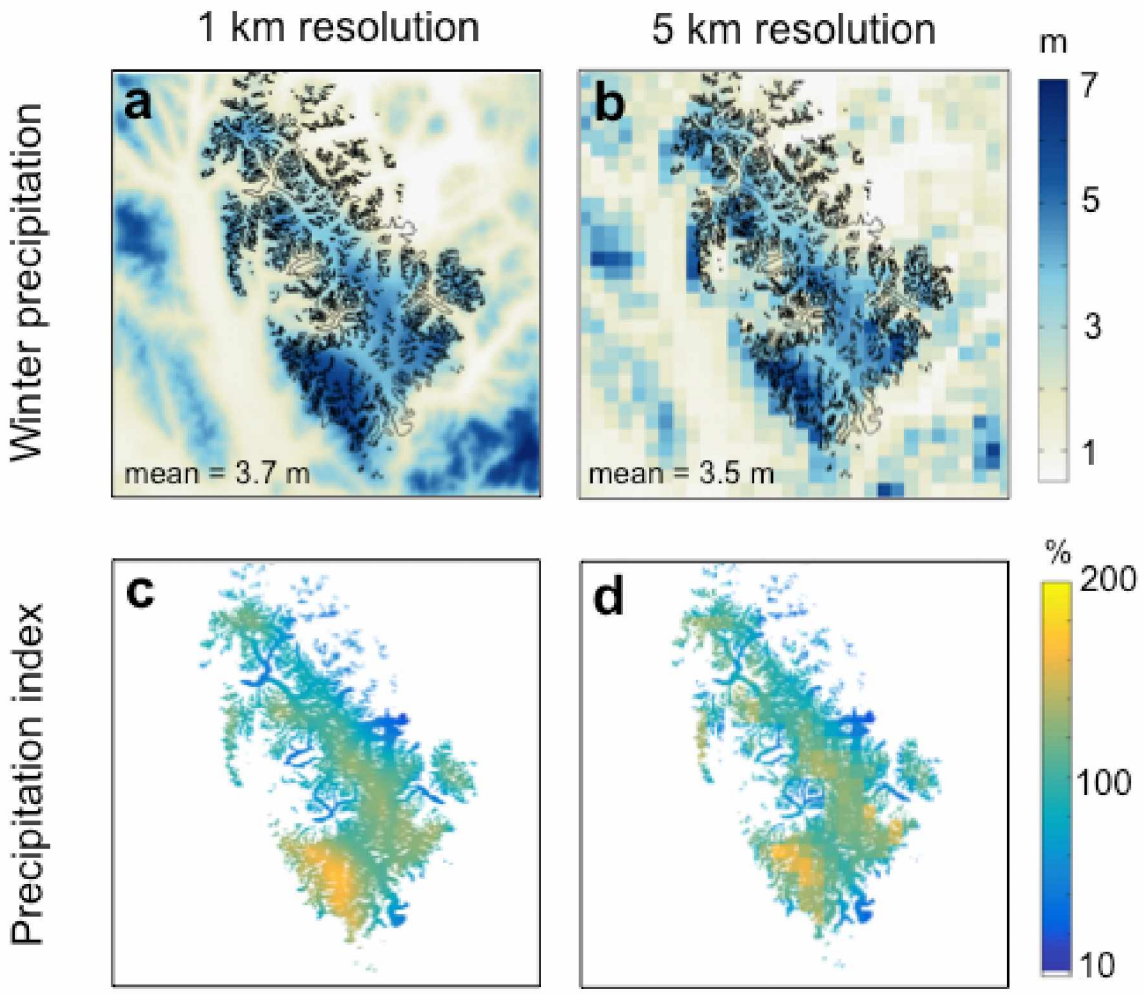

Figure 2.9. Modeled winter precipitation using different DEM resolutions. Modeled winter (October–March) precipitation (a, b) and precipitation index (d, e) averaged over 1979–2013 time period applying the LT model to the 1 km (a) and the 5 km (b) DEM. The precipitation index values indicate local deviations from the spatial mean and are computed as the ratio of each grid cell's time-averaged winter precipitation to the icefield-wide spatial winter precipitation mean, expressed as a percentage. The means noted in (a) and (b) refer to spatial means over all grid cells whose center lies inside the icefield outline. Thus the total area over which the spatial average is taken varies between the two cases.

input (Figure 2.10) . The icefield-wide spatial mean of average winter precipitation is 3.7 ± 1.1 m w.e and 2.4 ± 0.7 m w.e for the WRF and ERA-Interim forcings respectively. The precipitation index maps calculated using these mean values show that the precipitation pattern is similar between the two results (Figure 2.10).

The discrepancy between the amounts of average winter precipitation produced by the LT model when forced by different input climate datasets can be explained as follows. The LT model formulation vertically and horizontally averages the climate variable grids to solve for the precipitation solution. While the initial climate input is spatially variable in both the vertical (pressure level) and horizontal directions, the LT model equations are solved using the spatial mean of each grid at every time step. At every time step, these averaged quantities are slightly different for the two different climate datasets due to the difference in resolution and assumed topography of each dataset. In general, the higher resolution of the WRF grids and assumed topography means that more extreme values are represented in a given grid for any variable. This results in larger spatially averaged quantities compared to the average quantities calculated from the lower resolution ERA-Interim grids.

The WRF dataset leads to the application of the LT model in 86% of time steps compared to 79% for the ERA-Interim dataset. When the LT model is not applied, the precipitation field from input climate data set is used for that time step. Due to the coarse resolution of both climate datasets, the precipitation fields of the climate datasets underestimate precipitation compared to the LT model. The LT model is applied less often in the ERA-Interim case, indicating that the average winter precipitation more often includes time steps that are unaltered and underestimated precipitation fields from the original ERA-Interim dataset.

Despite the differences, the results from the WRF and ERA-Interim forcings both create improved precipitation fields that show the expected orographic precipitation pattern. In both cases, the LT model downscales the precipitation fields with a similar precipitation pattern that was previously unresolved in available climate data for the region. We cannot say whether forcing the LT model with the WRF or ERA-Interim dataset leads to more "realistic" precipitation fields due to the scarcity of total precipitation observations. However, the amount of average winter precipitation as calculated by the LT model is sensitive to the input climate dataset, in addition to DEM resolution and choice of v_{snow} and v_{rain} values. This indicates that similar LT model results can be achieved with either climate input dataset in conjunction with different combinations of DEM resolution, v_{snow}, and v_{rain} values.

2.7 Discussion

2.7.1 Precipitation Pattern and Amount

The LT model produces precipitation fields at a scale relevant for glacier mass balance modeling with a persistent precipitation pattern regardless of parameter combination, horizontal resolution,

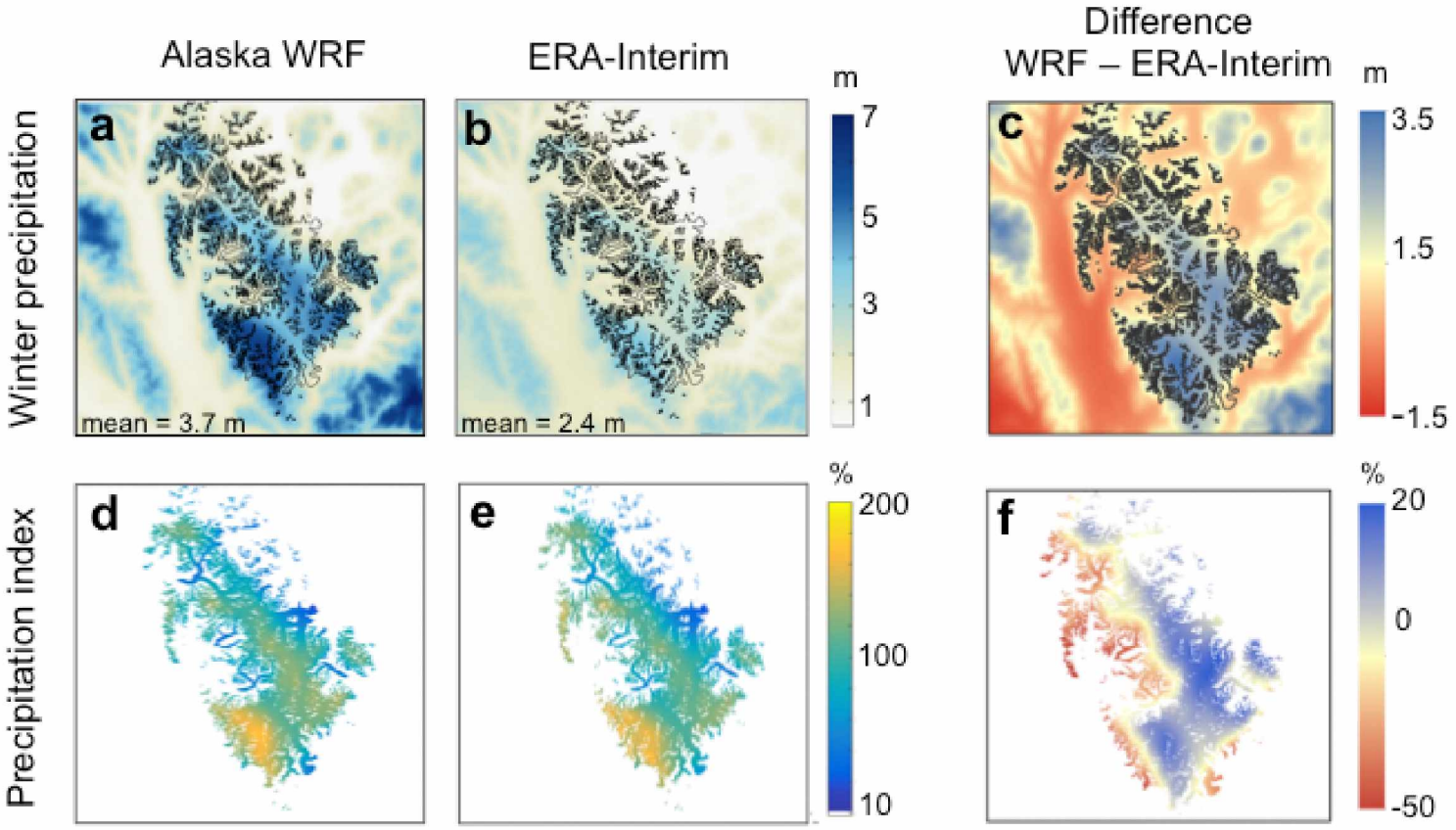

Figure 2.10. Average winter precipitation(1979-2013) from the LT model reference parameter set forced with WRF (a) and ERA-Interim (b) climate datasets. We show the difference between these two sets of results (c) where ERA-Interim results were subtracted from the WRF results. The precipitation pattern relative to the icefield-wide spatial mean for the WRF results (d) and ERA-Interim results (e) are shown. The precipitation pattern is expressed with precipitation index values defined as the ratio of the local average winter precipitation at each grid cell to the icefield-wide spatial mean of average winter precipitation, calculated as a percentage. The icefield-wide spatial mean for each set of results is noted. The difference between the precipitation patterns of the two sets of results is shown where the ERA-Interim precipitation index map was subtracted from the WRF precipitation index map.

and input data. The pattern reflects the increase in spatial resolution of the topograhy used in the LT model downscaling in comparison to the coarse resolution topography used by WRF and ERA-Interim. However, validating the precipitation pattern produced by the LT model over the Juneau Icefield is limited by the spatial extent of available observations. The net accumulation transect on Taku Glacier is perpendicular to the large scale orographic precipitation gradient over the icefield. Ideally, we could compare the LT model results with observations that parallel the orographic precipitation gradient.

While the precipitation pattern produced by the LT model is robust, the amount of precipitation is sensitive to model parameters, horizontal resolution, and input data. The icefield-wide spatial mean of average winter precipitation can be between 2.5 m w.e and 4.4 m w.e depending on choice of snow fall speed. The same parameter combination run at 1 km and 5 km resolution results in mean icefield winter precipitation values that can vary by more than 1.0 m The sensitivity of the results to these factors means that different combinations of model parameters, horizontal resolution, and input data can yield similar precipitation fields that show the same agreement with the available data.

The amount of total precipitation from the LT model results cannot be validated by the available observations which were taken in late July after significant melt had occurred. We accounted for this by deriving modeled net accumulation from the LT model results using a temperature-index model to calculate melt, which introduced a melt factor as a parameter that can vary the modeled net accumulation. LT model results that under or over estimate total precipitation can be made to match the available net accumulation observations by finding the "best choice" melt factor within a reasonable range. Thus, the model can show good agreement to the observations for the incorrect reasons. It is possible that a more sophisticated melt model could better constrain the amount of melt, but the total precipitation from the LT model results would still need to be validated.

Furthermore, the gradient of the modeled net accumulation is a function of the lapse rate used to downscale the temperature fields used in the melt calculation in addition to the gradient from modeled total accumulation. We assumed an invariant standard atmospheric lapse rate of Γ=0.0065 K m^{-1}, but a better agreement between model results and observations could be achieved with a lower value constant lapse rate as the average gradient of observed net accumulation is more shallow than the average modeled gradient. Additionally, other methods to calculate the lapse rate for temperature downscaling could have been used such as direct calculation of the lapse rate from the input climate data or a seasonally varying lapse rate.

The measurements capture local processes that are not considered by the LT model and thus some error is expected between the model results and measurements. We do not consider the process of refreezing of melt water or rain water within the snow or firn pack, as we assume that all melt and rain are not retained. Refreezing has been noted as significant processes in the upper firn zone of Taku

Glacier beginning at roughly 1350 m a.s.l. with most melt water being retained (Pelto et al., 2013). The observations that we used to validate the model results occur between 920 m a.s.l. and 1100 m a.s.l in the lower firn zone which experiences significant ablation and less refreezing, but ice lenses are often observed in the snow pits dug by JIRP, indicating that refreezing is present (Pelto et al., 2013). A more detailed analysis of snow density profiles would aid in estimating the error in the model results from not considering refreezing. Increased error in the model results from the exclusion of refreezing should be expected if additional observations from the upper firn zone are used in future studies.

2.7.2 Suggested Precipitation Gauge Locations

Previous studies have used relatively dense networks of precipitation gauge measurements from upper elevations of the study area to validate the LT model results of total precipitation amount and pattern directly before comparing the results to glaciological data. These types of observations do not exist for the Juneau Icefield. However, the results of the LT model can inform where precipitation gauge measurements should occur in order to capture the large scale heterogeniety of precipitation on the icefield, constrain precipitation amounts to realistic values, and to more thoroughly validate the LT model results.

Figure 2.11 shows four locations of suggested precipitation gauges that would be ideal for LT model validation. These locations are at the local maxima and minima average winter precipitation locations from the results of the LT model reference run. A precipitation gauge at the divide between Mendenhall Glacier and Taku Glacier could be used in conjunction with precipitation gauges close to sea level in Juneau to validate the precipitation gradient in the southwestern corner of the icefield and validate the local precipitation maximum at this location. The LT model shows a precipitation minimum on the upper main branch of Taku Glacier. A precipitation gauge at this location would allow this precipitation minimum to be confirmed and improve the comparison of model results to the net accumulation transect. Additionally, JIRP Camp 10 is at this location, allowing for access and maintenance of a precipitation gauge in this location. A precipitation gauge at the divide between Gilkey Glacier and Llewellyn Glacier would confirm the second local precipitation maximum on the icefield. A precipitation gauge at this location used in combination with the fourth suggested location at the terminus or lower elevations of Llewellyn Glacier, would allow for the leeside precipitation gradient to be confirmed.

There are small scale patterns in the modeled average winter precipitation field in the northwest (Meade Glacier) and southeast (East Twin Glacier) corners that would be ideal to validate with precipitation gauge measurements as well. However, these areas are of less consequence to the overall icefield mass balance than the other precipitation gauge locations suggested. Additionally, there are fewer, if any at all, glaciological observations in these areas that could be used to further validate and

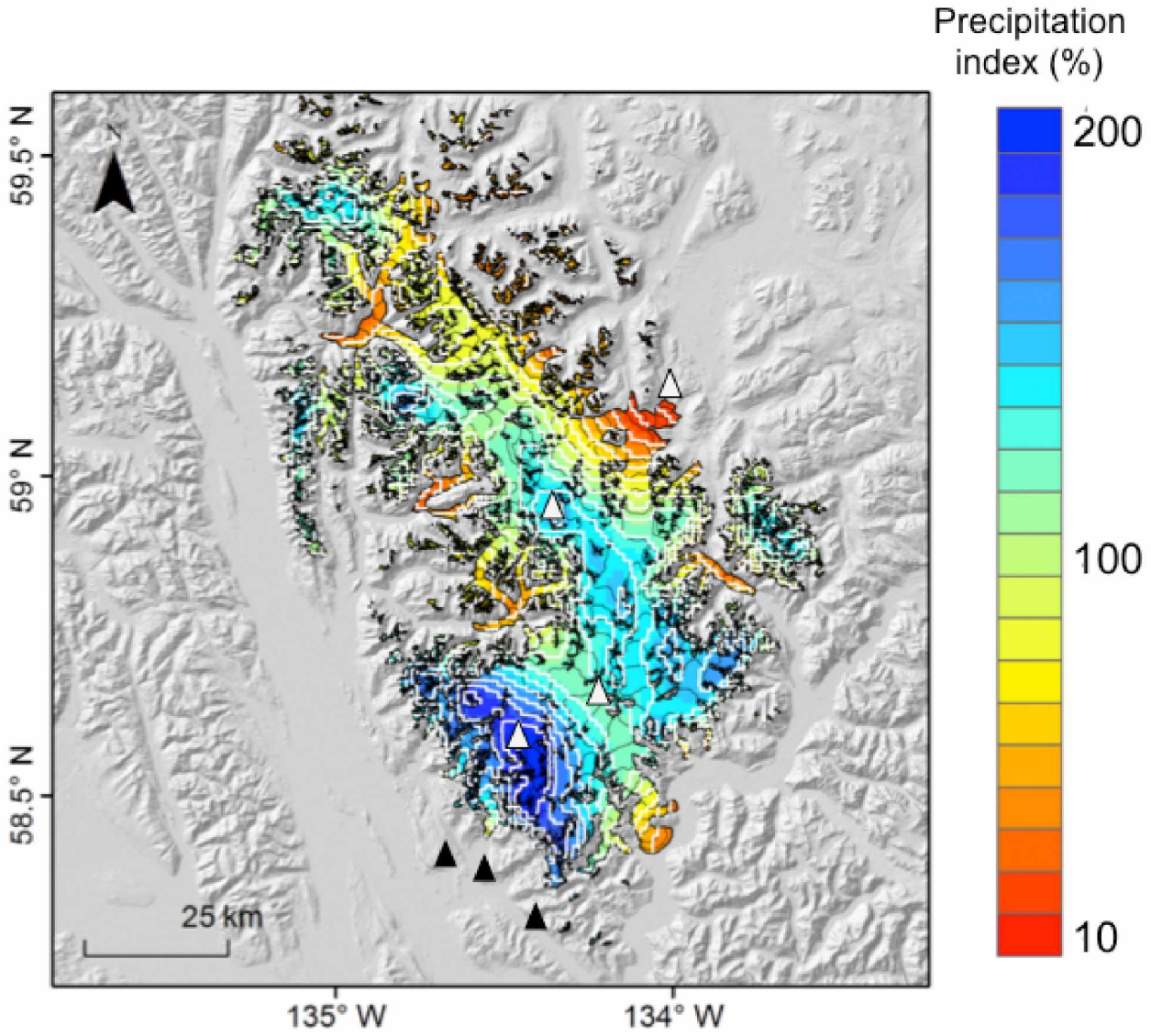

Figure 2.11. Winter precipitation index map for the Juneau Icefield and suggested precipitation gauge locations.The index map is calculated from the LT model reference run results. The precipitation index values represent the ratio of the local average winter precipitation at each grid cell to the icefield-wide spatial mean of average winter precipitation expressed as a percentage. The icefield-wide spatial mean of average winter precipitation for the reference run is 3.7 m. The precipitation index map is also illustrated with the white contours (at intervals of 10%). The black contour lines illustrate the topography (at intervals of 100 m). Note that the precipitation index patten deviates from the distribution of terrain elevation, especially on the western side of the icefield. The white triangles show suggested locations for precipitation gauges that would better validate the LT model results. The locations of the gauges are based on the local minima and maxima of average winter precipitation. Existing precipitation gauges close to sea level in Juneau are shown (black triangles).

analyze the LT model results.

2.7.3 Precipitation Index Map

Snow accumulation on glaciers often exhibits a persistent pattern from year-to-year and accumulation index maps have been used to describe this pattern for input in distributed mass balance and hydrological modeling (Schuler et al., 2008). The accumulation at each time step can be calculated by adding an anomaly to the mean pattern described by the accumulation index map or by using the accumulation index map as a map of weighting factors to distribute a point value. The consistent pattern produced by the LT model and the uncertainty of the precipitation amount suggests that an accumulation index map may be a practical approach for further mass balance modeling of the Juneau Icefield. The accumulation index map approach also decreases computational cost for interfacing the LT model with a mass balance model.

Following the approach of Schuler et al. (2008) we derive a winter precipitation index map for the Juneau Icefield using the LT model (Figure 2.11). We consider total precipitation, not just snow accumulation, as the fraction of snow and rain would be dealt with in a more sophisticated mass balance modeling scheme. The average winter (October-March) precipitation for the model period (1979-2013) is calculated using the reference run parameters at 1 km resolution downscaled from the WRF climate data. The precipitation index values represent the ratio of the local average winter precipitation at each grid cell to the icefield-wide spatial mean of average winter precipitation expressed as a percentage. Values larger than 100% indicate average winter precipitation is larger than the mean and vice versa. While there is a general trend that precipitation index increases with elevation, there are specific areas of deviation, which would not be resolved if the common lapse rate approach was used to downscale precipitation.

Functionally, this precipitation index map could be used in conjunction with a parameter contained within the mass balance model scheme that would increase or decrease precipitation amount across the domain while maintaining the pattern specified by the index map. This parameter would be a tuning parameter in addition to degree-day factors, but it has potential to be constrained more than the LT model parameters as it would be included in a more sophisticated distributed mass balance modeling scheme.

Chapter 3
Conclusions and Future Directions

3.1 Conclusions

Global and regional climate models perform at a resolution that is too coarse to capture local orographic precipitation patterns in complex terrain. For any distributed glacier mass balance modeling, developing precipitation input at the appropriate scale is a necessary step. This has commonly been done by applying an elevation-dependent lapse rate to the study domain for both point data and coarse scale gridded global or regional climate model output. For areas with complex terrain and significant orographic precipitation, such as the Juneau Icefield, this method cannot appropriately capture the precipitation pattern as precipitation does not linearly scale with elevation everywhere. Instead, a rain shadow pattern exists where the windward side of a mountain range receives significantly more precipitation than the leeward side at the same elevation. We assessed the ability of a linear theory of orographic precipitation model (LT model) as a physically-based, intermediate complexity tool that can be used to downscale coarse gridded global or regional climate data for the purposes of glacier mass balance modeling. The Juneau Icefield was used as a study site to address previous challenges of mass balance modeling related to the representation of orographic precipitation in the precipitation input data. Accurate mass balance modeling of the Juneau Icefield is necessary for future studies aimed at assessing runoff and regional impacts of glacier mass loss.

We compared five years of net accumulation observations to modeled net accumulation derived from the established LT model reference run results, combined with a temperature-index model to account for melt over the observation time period. The modeled net accumulation showed an agreement of $r^2 = 0.89$ to the observations when the average net accumulation of the five years was calculated. The LT model produced winter precipitation fields with the expected orographic precipitation pattern previously unresolved in precipitation fields for the area. Due to the scarcity of observations, we were unable to directly validate the total precipitation results of the LT model. We instead performed a series of sensitivity experiments to assess the robustness of the LT model results. We varied the LT model parameters of snow fall speed and rain fall speed, the horizontal resolution of the underlying DEM, and the climate input data. The pattern of winter precipitation persisted in the results of the sensitivity experiments while the amount of winter precipitation varied with these factors and was most influenced by the choice of snow fall speed. We showed that different combinations of LT model parameters, DEM resolution, and climate input data can produce similar LT model results.

Based on the persistence of the precipitation pattern produced by the LT model results and the uncertainty in precipitation amount, we calculated a winter precipitation index map that could be used to improve mass balance modeling efforts of the Juneau Icefield. While this map shows the expected orographic precipitation pattern for the area, it has not been fully validated due to the lack of obser-

vations. From the LT model reference run results, we suggested locations for potential precipitation gauges that would improve parameter identification and validation of the LT model results.

3.2 Using a Different LT Model Parameterization

There are several different implementations of the LT model that have been used for glaciological applications. The original model proposed by Smith and Barstad (2004) was forced by user-specified meteorological constants that described the climate and atmospheric state. More recent versions of the LT model compute domain-averaged values of meteorological variables that vary with each time step from gridded global or regional climate model data to force the LT model. However, the cloud microphysics timescale, τ, describing the formation and fall out of hydrometeors, and the atmospheric stability parameter, N_m, often remained user-specified constants the values of which were determined by calibrating the LT model results to observations.

The implementation of the LT model used in this study parameterized N_m so that it was calculated directly from the climate data and varied with each time step. τ was derived from the climate data and hydrometeor fall speed, which was calculated using two parameters, snow fall speed and rain fall speed. This is a unique parameterization of τ not used in previous glaciological applications of the LT model. Crochet (2012) eliminated the need for any tuning parameters by calculating hydrometeor fall speed as a function of temperature in the moist layer. It was shown that this did not significantly improve the agreement between the LT model results and observations compared with using a constant value of τ. The parameterization implemented here, with snow fall speed and rain fall speed, lies between these two approaches. The ability of the parameters to adjust the modeled precipitation amount may be a desirable trait to obtain the best model agreement with observations. However, in areas with few or no observations, it may be better to implement the parameterization in Crochet (2012). It would be worth investigating whether the Crochet (2012) parameterization improves or diminishes the LT model results for the Juneau Icefield.

3.3 Precipitation Analysis

We assessed the results of the LT model in terms of average winter precipitation pattern and the icefield-wide spatial mean of winter precipitation. These are two characteristics of precipitation that were appropriate to consider for our study based on our available glaciological observations. Previous studies also evaluated the ability of the LT model to simulate individual storms, extreme precipitation events, and frequency of precipitation events. This evaluation is only possible if there are precipitation gauge measurements. If precipitation gauge measurements were made available in the future, evaluating the LT model in this manner would be a natural next step.

3.4 An Adjoint Model for Sensitivity Analysis

We suggested four potential locations of precipitation gauges across the icefield that would allow for improved calibration and validation of LT model results. These locations represent the local maxima and minima of the average winter precipitation pattern across the icefield. The precipitation observations at the suggested stations as well as the precipitation gradients between the suggested stations, would allow for a thorough validation of the LT model results. While these are important locations for describing the precipitation pattern and amount, these locations may not be the most sensitive to changes in model parameters. For improved model validation and parameter determination, it would be ideal to have observations from the locations of the precipitation pattern most sensitive to the model parameters.

These locations could be determined by an adjoint model, a powerful approach used in meteorology and oceanography for sensitivity analysis and parameter identification (Errico, 1997). The sensitivity analysis in this study evaluated the impact of changes to the input parameters on the LT model output. The LT model was run forward in time to do this. In contrast, the adjoint equations of the LT model would describe the evolution of sensitivity backward in time and can be used to compute the sensitivity of the output of a model to all input parameters (Errico, 1997; Talagrand and Courtier, 1987; Courtier and Rabier, 1997). One result of an adjoint model is a spatial pattern of sensitivity and this could be used to indicate the optimal locations of precipitation gauges for efficient parameter determination and model validation of the LT model.

Adjoint models for sensitivity analysis have been used for decades with complex, nonlinear regional weather forecasting and global climate models with hundreds of parameters. More recently, the cryosphere community has used adjoint models for investigating the sensitivity of ice sheet models (Heimbach and Bugnion, 2009). In comparison to climate models and ice sheet models, the LT model is simple with linear equations and several parameters. It would seem that developing an adjoint model for the LT model should be possible and this would be a fruitful future direction of study.

3.5 LT Model Applications in Alaska

The LT model could be used in other regions of Alaska where orographic precipitation is dominant and WRF downscaling is insufficient due to complex topography, mainly Southeast and Southcentral Alaska. All of Southeast Alaska could be considered as a model domain, though modifications may have to be made to the model implementation and subdomains would have to be delineated. Lack of precipitation gauges at high elevations for validation would again pose challenges so glaciological data would need to be used. If the LT model were used in conjunction with a glacier runoff model or a hydrology model, hydrograph datasets could potentially be used to calibrate the LT model in addition

to glaciological measurements and precipitation gauge measurements. There is significant potential for the LT model to improve glacier mass balance, runoff, and hydrology modeling for regions with complex topography and orographic lifting in Alaska and elsewhere, and it should become a widely used tool for downscaling precipitation input for these purposes.

References

Barstad, I. and R. B. Smith (2005). Evaluation of an orographic precipitation model. *Journal of Hydrometeorology 6*(1), 85–99.

Bieniek, P., U. S. Bhatt, J. E. Walsh, T. S. Rupp, J. Zhang, J. R. Krieger, and R. Lader (2016). Dynamical downscaling of ERA-Interim temperature and precipitation. *Journal of Applied Meteorology and Climatology 55*(3), 635–654.

Braithwaite, R. J. (2008). Temperature and precipitation climate at the equilibrium-line altitude of glaciers expressed by the degree-day factor for melting snow. *Journal of Glaciology 54*(186), 437–444.

Courtier, P. and F. Rabier (1997). The use of adjoint equations in numerical weather prediction. *Atmosphere-Ocean 35*(1), 303–322.

Crochet, P. (2012). High resolution precipitation mapping in Iceland by dynamical downscaling of ERA-40 with a linear model of orographic precipitation. Technical Report VI 2012-003, Iceland Meteorological Office, Reykjavik, Iceland. URL http://en.vedur.is/about-imo/publications/2012/, accessed June 2015.

Crochet, P., T. Jóhannesson, T. Jónsson, O. Sigurdsson, H. Björnsson, F. Pálsson, and I. Barstad (2007). Estimating the spatial distribution of precipitation in Iceland using a linear model of orographic precipitation. *Journal of Hydrometeorology 8*(6), 1285–1306.

Daly, C., R. P. Neilson, and D. L. Phillips (1994). A statistical-topographic model for mapping climatological precipitation over mountainous terrain. *Journal of Applied Meteorology 33*, 140–158.

Dee, D. P., S. M. Uppala, A. J. Simmons, P. Berrisford, P. Poli, S. Kobayashi, U. Andrae, M. A. Balmaseda, G. Balsamo, P. Bauer, P. Bechtold, A. C. M. Beljaars, L. van de Berg, J. Bidlot, N. Bormann, C. Delsol, R. Dragani, M. Fuentes, A. J. Geer, L. Haimberger, S. B. Healy, H. Hersbach, E. V. Hólm, L. Isaksen, P. Kå llberg, M. Köhler, M. Matricardi, A. P. McNally, B. M. Monge-Sanz, J.-J. Morcrette, B.-K. Park, C. Peubey, P. de Rosnay, C. Tavolato, J.-N. Thépaut, and F. Vitart (2011). The ERA-Interim reanalysis: configuration and performance of the data assimilation system. *Quarterly Journal of the Royal Meteorological Society 137*(656), 553–597.

Durran, D. R. and J. B. Klemp (1982). On the Effects of Moisture on the Brunt-Väisälä Frequency. *Journal of the Atmospheric Sciences 39*(1), 2125–2158.

Errico, R. M. (1997). What Is an Adjoint Model? *Bulletin of the American Meteorological Society 78*(11), 2577–2591.

Heimbach, P. and V. Bugnion (2009). Greenland ice-sheet volume sensitivity to basal, surface and initial conditions derived from an adjoint model. *Annals of Glaciology 50*(52), 67–80.

Heymsfield, A. (2007). Refinements to ice particle mass dimensional and terminal velocity relationships for ice clouds. Part II: Evaluation and parameterizations of ensemble ice particle sedimentation velocities. *Journal of Atmospheric Sciences 64*(4), 1068–1088.

Hock, R. and B. Holmgren (2005). A distributed surface energy-balance model for complex topography and its application to Storglaciären, Sweden. *Journal of Glaciology 51*(172), 25–36.

Hood, E. and L. Berner (2009). Effects of changing glacial coverage on the physical and biogeochemical properties of coastal streams in southeastern Alaska. *Journal of Geophysical Research: Biogeosciences 114*(3), 1–10.

Huss, M. and R. Hock (2015). A new model for global glacier change and sea-level rise. *Frontiers in Earth Science 3*(September), 1–22.

Jarosch, A. H., F. S. Anslow, and G. K. C. Clarke (2012). High-resolution precipitation and temperature downscaling for glacier models. *Climate Dynamics 38*(1), 391–409.

Jóhannesson, T., G. Adalgeirsdóttir, H. Björnsson, and P. Crochet (2007). Effect of climate change on hydrology and hydro-resources in Iceland. Technical Report OS-2007/011, National Energy Authority–Hydrological Service, Reykjavík, Iceland.

Kienholz, C., S. Herreid, J. L. Rich, A. Arendt, R. Hock, and E. W. Burgess (2015). Derivation and analysis of a complete modern-date glacier inventory for Alaska and northwest Canada. *Journal of Glaciology 61*(227), 403–420.

Locatelli, J. D. and P. V. Hobbs (1974). Fall speeds and masses of solid precipitation particles. *Journal of Geophysical Research 79*(15), 2185–2197.

Machguth, H., F. Paul, S. Kotlarski, and M. Hoelzle (2009). Calculating distributed glacier mass balance for the Swiss Alps from regional climate model output: A methodical description and interpretation of the results. *Journal of Geophysical Research Atmospheres 114*(19), 1–19.

O'Neel, S., E. Hood, L. Bidlack, S. W. Fleming, M. L. Arimitsu, A. Arendt, E. Burgess, C. J. Sergeant, H. Beaudreau, K. Timm, G. D. Hayward, J. H. Reynolds, and S. Pyare (2015). Icefield-to-Ocean linkages across the Northern Pacific Coastal Temperate Rainforest ecosystem. *BioScience 65*(5), 1–14.

Pelto, M., J. Kavanaugh, and C. McNeil (2013). Juneau Icefield mass balance program 1946-2011. *Earth System Science Data 5*(2), 319–330.

Radić, V., A. Bliss, C. Beedlow, R. Hock, E. Miles, and J. G. Cogley (2014). Regional and global projections of twenty-first century glacier mass changes in response to climate scenarios from global climate models. *Climate Dynamics 42*(1-2), 37–58.

Radić, V. and R. Hock (2011). Regionally differentiated contribution of mountain glaciers and ice caps to future sea-level rise. *Nature Geoscience 4*(2), 91–94.

Schuler, T. V., P. Crochet, R. Hock, M. Jackson, and I. Barstad (2008). Distribution of snow accumulation on the Svartisen ice cap, Norway, assessed by a model of orographic precipitation. *Hydrological Processes 22*, 3998–4008.

Sinclair, M. R. (1994). A diagnostic model for estimating orographic precipitation. *Journal of Applied Meteorology 33*(10), 1163–1175.

Skamarock, W., J. Klemp, J. Dudhi, D. Gill, D. Barker, M. Duda, X.-Y. Huang, W. Wang, and J. Powers (2008, June). A Description of the Advanced Research WRF Version 3. Technical Report NCAR/TN-475+STR, Mesoscale and Microscale Meteorology Division, National Center for Atmospheric Research, Boulder, Colorado. URL http://www2.mmm.ucar.edu/wrf/users/docs/arw_v3.pdf, accessed June 2015.

Smith, R. B. and I. Barstad (2004). A Linear Theory of Orographic Precipitation. *Journal of the Atmospheric Sciences 61*(12), 1377–1391.

Stone, P. H. and J. H. Carlson (1979). Atmospheric Lapse Rate Regimes and Their Parameterization. *Journal of Atmospheric Sciences 36*, 415–423.

Talagrand, O. and P. Courtier (1987). Variational Assimilation of Meteorological Observations With the Adjoint Vorticity Equation. I: Theory. *Quarterly Journal of the Royal Meteorological Society 113*(478), 1311–1328.

Yuter, S. E., D. E. Kingsmill, L. B. Nance, and M. Löffler-Mang (2006). Observations of precipitation size and fall speed characteristics within coexisting rain and wet snow. *Journal of Applied Meteorology and Climatology 45*(10), 1450–1464.

Ziemen, F., R. Hock, A. Aschwanden, C. Khroulev, C. Kienholz, A. K. Melkonian, and J. Zhang (2016). Modeling the evolution of the Juneau Icefield between 1971 and 2100 using the Parallel Ice Sheet Model (PISM). *Journal of Glaciology 62*(231), 199–214.